NACA RM A53I01

RESEARCH MEMORANDUM

APPLICATIONS OF AUXILIARY AIR INJECTORS TO SUPERSONIC WIND TUNNELS

By Joseph M. Spiegel, Robert U. Hofstetter, and Donald M. Kuehn

Ames Aeronautical Laboratory
Moffett Field, Calif.

NATIONAL ADVISORY COMMITTEE FOR AERONAUTICS

WASHINGTON

November 25, 1953
Declassified August 9, 1954

NATIONAL ADVISORY COMMITTEE FOR AERONAUTICS

RESEARCH MEMORANDUM

APPLICATIONS OF AUXILIARY AIR INJECTORS TO SUPERSONIC WIND TUNNELS

By Joseph M. Spiegel, Robert U. Hofstetter, and Donald M. Kuehn

SUMMARY

Adverse effects of high compression-ratio requirements for supersonic wind tunnels are discussed, together with the use of second throats for alleviating these effects. The application of an air injector as an auxiliary to a conventional wind tunnel is explained, and a one-dimensional theory and experimental data are presented to demonstrate the feasibility of the device for reducing starting and running compression ratios, but at the expense of an increase in power requirements. For a continuous-operation wind tunnel of variable Mach number and conventional compressor drive-unit, the installation of an air-injector system can extend the Mach number range without surging the compressor and can reduce starting difficulties. These results are obtainable without any additional pumping equipment. For a blowdown-type wind tunnel with a divergent diffuser, the installation of an air-injector system can reduce starting loads, increase running time, and raise the maximum operating Mach number. It should not be used when power is of primary concern, except possibly as a device for controlling boundary layer at mass ratios less than 0.2. A recommended design procedure is provided for the application of the auxiliary-injector principle to supersonic wind tunnels.

INTRODUCTION

In the design of supersonic wind tunnels, a primary problem is the large loss of total pressure which results from the deceleration of supersonic flow in the diffuser. This deceleration occurs in the form of strong shock waves which, in turn, produce additional losses as a result of their interaction with the boundary layer of the wind-tunnel diffuser. Thus, the wind-tunnel drive system must provide sufficient compression ratio (ratio of settling-chamber to diffuser-exit total

pressure) to overcome these shock losses. For continuous-operation wind tunnels, high compression ratios result in excessive power requirements and large pumping equipment. In the case of intermittent-operation wind tunnels (blowdown) with atmospheric discharge, high compression ratios result in short running periods, restriction of maximum Mach number, and high oscillatory starting and stopping loads on the wind-tunnel model. These abnormal loads on the model are a result of unsteady, asymmetric flow separation from the walls of the wind-tunnel nozzle during the starting and stopping processes.

The variable second throat, which is one device known to reduce the compression ratio required, can do so, at a given Mach number, only after the wind tunnel has been "started"; that is, after the terminal shock waves have been "trapped" just downstream of the minimum area of the second throat. In order to start a wind tunnel with a variable second throat, the tunnel must have either a continuously adjustable nozzle to permit lower Mach number starting or sufficient compression ratio available to overcome the large shock losses that occur as the terminal shock system passes through the test section. Other methods of starting second-throat tunnels have been studied (refs. 1 and 2) but have not been completely proven in practice as yet.

For an intermittent-type wind tunnel incapable of rapid changes in nozzle Mach number, a source of high compression ratio for starting a variable second throat does not solve the problem of high starting loads on the model. In fact, these loads would be expected to vary approximately in proportion to the dynamic pressure for a given starting time.

For continuous-operation wind tunnels there is a problem other than high power requirements that must be considered. This is the problem of matching the compressor flow quantities to those required by the wind-tunnel nozzle over a large range of Mach numbers. The maximum Mach number at which a wind tunnel can operate is determined by either of two factors. The first is the point where the minimum compression ratio required by the tunnel equals that available from the compressor, and the second is the compressor-surge limit which terminates the operating range at low flow rates. Compressor surge can be forestalled by bypassing air around the throat of the test-section nozzle in sufficient quantities to permit the compression-ratio limitation to be reached. It can be shown that a variable second throat makes the matching problem more difficult.

An air injector, as an auxiliary to conventional wind tunnels, presents the possibility of alleviating some of the difficulties just discussed. For an intermittent-operation wind tunnel, a reduction in the required starting compression ratios by use of an injector would be expected to lower the starting and stopping loads without the need for a rapidly adjustable nozzle. For the continuous-operation wind tunnel,

the auxiliary air injector presents some attractive features on the basis of the incompatibility between conventional air-compressor characteristics and supersonic-wind-tunnel requirements. If the air that must be bypassed to prevent compressor surge is channeled to an auxiliary injector, an improvement in both starting and running characteristics of the wind tunnel would be expected.

In this report a one-dimensional analysis of the auxiliary-injector principle is presented, together with some experimental results. Examples are given that demonstrate the improvement in operating characteristics of both intermittent- and continuous-operation wind tunnels from the standpoint of compression-ratio reduction.

SYMBOLS

a sonic velocity, ft/sec

A cross-sectional area, sq ft

C any constant

c_p specific heat at constant pressure, $ft^2/sec^2/^oF$

K stagnation pressure ratio, $\frac{p_{t_J}}{p_{t_o}}$

m mass-flow ratio, $\frac{\text{injector mass flow}}{\text{test-section mass flow}}$

M Mach number

P power, ft-lb/sec

p static pressure, lb/sq ft abs

Q flow quantity, based on compressor intake conditions, cu ft/min

r compression ratio

r_f correction factor, $\frac{r_{experiment}}{r_{theory}}$

R perfect-gas constant, $ft^2/sec^2/^oF$

T	temperature, ^{o}F abs
V	velocity, ft/sec
Y	$(r^{0.286} - 1)$
γ	ratio of specific heats, $\frac{c_p}{c_v} = 1.400$
ρ	mass density, slugs/cu ft

Subscripts

c	conventional wind tunnel (no auxiliary injection)
D	discharge of compressor
e	exit of divergent diffuser
J	injector
m	mixing losses
ns	normal shock
N	main stream (through test section)
opt	optimum
T	total, auxiliary-injector wind tunnel
t	stagnation conditions
w	mixing-tube wall
o	station a (fig. 1), upstream of normal shock
1	station a (fig. 1), downstream of normal shock
2	station c (fig. 1), main stream (through test section)
3	station d (fig. 1), end of mixing region
4	station e (fig. 1), upstream of terminal shock
5	station e (fig. 1), downstream of terminal shock

Superscripts

* condition when M = 1

' downstream of normal shock

" downstream of injection station when pressures have equalized

ANALYSIS

For purposes of analysis, an idealized two-dimensional installation of an auxiliary air injector is shown in figure 1. The arrangement consists of an injector nozzle and isentropic contraction placed just downstream of the test section, followed by a constant-area mixing region, downstream isentropic contraction, and a subsonic diffuser. The solid outline in the figure denotes the wall position for nonviscous flow and the dotted lines, the wall position after compensation for boundary layer.

The actual mixing process of the two streams is not fully understood (ref. 3). Therefore, a one-dimensional analysis has been used in this report and the results compared with experiment for the purpose of obtaining empirical relations to use for future designs.

Numerous treatments have been made of conventional ejectors and induction wind tunnels by the one-dimensional method (e.g., refs. 4 and 5), but the presentations of final results all differ somewhat, due to the specific objectives involved in each case. In Appendixes A and B such a one-dimensional analysis has been made, based on the idealized auxiliary air injector shown in figure 1. The assumptions made in this analysis are:

1. Complete mixing is obtained at station d.

2. All flows are isentropic except for adiabatic flows in the mixing region and through normal shock waves.

3. The velocities are negligibly small in the wind tunnel and injector settling chambers, and at the end of the subsonic diffuser.

4. All flows are frictionless.

5. The total temperature ratio (T_{t_J}/T_{t_o}) is unity. (This eliminates

one independent variable and is a good assumption for all experimental data presented herein.)

The independent variables for a given value of M_o are:

1. mass-flow ratio (m)
2. injection Mach number (M_J)
3. total pressure ratio between injector and tunnel streams (K)
4. contraction ratio of tunnel stream before mixing (A_1/A_2)
5. contraction ratio of tunnel stream after mixing (A_3/A_4)

Since a normal shock wave is stable in a diverging passage, it is apparent from figure 1 that the normal shock will stand upstream of station a or downstream of station e. The upstream position is called the starting condition and the downstream, the running condition. The possibility of a normal shock wave in the mixing region is not within the scope of this analysis.

It is seen from the integral term of the momentum equation (A8) in Appendix A that an infinite number of solutions are possible, depending on the shape of the mixing-tube walls. However, only constant-area and constant-pressure mixing are amenable to simple solution and will be presented here. The object of this analysis is to obtain expressions for the compression ratio ($r = p_{t_o}/p_{t_e}$) in terms of M_o and the independent variables.

Summary of Final Equations[1]

Equations for constant-area mixing.- For constant-area mixing ($A_3 = A_2 + A_J$), the compression ratio required, due to mixing and normal shock losses, from equations (A7) and (A14) of Appendix A is

$$r = \frac{r_m}{\left(\frac{p_t'}{p_t}\right)_4} = \frac{\left(\frac{A^*}{A}\right)_3 \left[\frac{A_2}{A_1} + \frac{m}{K}\,\frac{(A^*/A)_o}{(A^*/A)_J}\right]}{\left(\frac{A^*}{A}\right)_o (1+m) \left(\frac{p_t'}{p_t}\right)_4} \tag{1}$$

[1]In this report the ratios (A^*/A), (ρ/ρ_t), (T/T_t), (a/a_t), (p/p_t), and (p_t'/p_t) represent the usual one-dimensional flow equations which are functions only of the local Mach number at the point designated by the subscript. They are redefined in Appendix A for convenience.

and M_4 is related to M_3 by equation (A15). From equation (A10), M_3 is determined by

$$f(M_3) = \frac{1}{1 + m} \left[f(M_2) + m f(M_J) \right] \tag{2}$$

and $f(M_2)$ and $f(M_J)$ have the same form as $f(M_3)$. For each value of $f(M)$, there is a supersonic and a subsonic value of M which are related by one-dimensional normal-shock equations. The reciprocal of $f(M)$ times a constant is tabulated in reference 6 for Mach numbers of 0 to 5. Because this constant cancels from equation (2), these reciprocal values can be used directly.

For the starting condition it is to be noted that $(p_t'/p_t)_4 = 1$ in equation (1), and the subsonic value of M_3 from $f(M_3)$ must be used in equation (2). The value of M_2 is obtained by use of equations (A11) and (A12).

Equations for constant-pressure mixing.- In the case of constant pressure along the mixing-tube wall ($p_3 = p_J$), station d coincides with e in figure 1 because the mixing tube must change area to maintain constant pressure at the wall. The continuity equation from equations (B1) and (A13) gives the compression ratio as

$$r = \frac{r_m}{\left(\frac{p_t'}{p_t}\right)_3} = \frac{\left(\frac{p}{p_t}\right)_3}{K\left(\frac{p}{p_t}\right)_J} \frac{1}{\left(\frac{p_t'}{p_t}\right)_3} \tag{3}$$

From equation (B5), M_3 is determined by (for running condition $(p_t'/p_t)_0 = 1$)

$$f(M_3) = \frac{\left(\frac{A_2}{A_1}\right)\left(\frac{a}{a_t}\right)_0}{\gamma M_0 \left(\frac{p}{p_t}\right)_0 (1+m)} \left[\left(\frac{p}{p_t}\right)_2 (\gamma M_2^2 + 1) + K\left(\frac{p}{p_t}\right)_J \left(\gamma \frac{A_J}{A_2} M_J^2 - 1\right) \right] \tag{4}$$

The contraction ratio, $(A_2 + A_J)/A_3$, is given by equation (B7)

$$\frac{A_2 + A_J}{A_3} = \frac{K\left(\frac{p}{p_t}\right)_J \left(\frac{A^*}{A}\right)_3}{\left(\frac{p}{p_t}\right)_3 \left(\frac{A^*}{A}\right)_0} \left[\frac{\frac{A_2}{A_1} + \frac{m}{K} \frac{(A^*/A)_0}{(A^*/A)_J}}{(1 + m)} \right] \tag{5}$$

Results and Discussion of Analysis

Comparison of constant-area and constant-pressure mixing.- In order to make a valid comparison, it is necessary for the two cases to have equal downstream contraction ratios. This is done by inserting the results of equation (B3) (after solving for A_1/A_3) into equation (A15) (with A_3 set equal to A_4) to determine the proper value of M_4. Such a comparison is made in figure 2(a) for the simplified running case of $A_2 = A_1$, $M_0 = 3$, $M_J = 2$, and where (A_1/A_4) for constant area equals (A_1/A_3) for constant pressure. It is seen that the constant-area condition yields lower compression ratios, which is in agreement with reference 3. At a mass ratio of zero, where no mixing losses can occur, the constant-area case represents an isentropic contraction ($r_m = 1$), but the constant-pressure case does not. The latter condition is indicative of a shock wave which must emanate from the wall discontinuity at station c in order to satisfy the stipulation that $p_J = p_3$ at $m = 0$. It should be noted that $p_2 = p_3$ can be assumed in the constant-pressure solution. This approach leads to $r_m = 1$ when $m = 0$ but, for the conditions assumed in figure 2, contraction ratios less than unity result. This leads to r values much higher than shown in figure 2(a). Furthermore, it is obvious that, for $M_J = M_2$ and $K = 1$, a trite solution results.

Figure 2(b) gives the variation of contraction ratio for constant-pressure mixing as a function of mass ratio. For the analogous constant-area solution it can be shown that none of these contraction ratios would permit starting. Consideration of the starting case for the constant-pressure solution indicates that it is not possible to start an auxiliary-injector wind tunnel with a constant-pressure mixing tube. This can be seen from equation (B5) from which it can be shown that

$$\left(\frac{p}{p_t}\right)_2 \left(\frac{p_t'}{p_t}\right)_0 (\gamma M_2^2 + 1) = \left(\frac{p}{p_t}\right)_0 (\gamma M_0^2 + 1)$$

Therefore, since $f(M_3)$ in equation (4) is single valued, it is apparent that only one solution is possible, and the assumption of a normal shock at station a with M_3 supersonic denotes effectively an $M = 1$ region in the mixing tube.

From the foregoing discussion it is apparent that only the constant-area condition is adaptable to the analysis of specific configurations, both starting and running, because of the independent selection of downstream contraction. Therefore, the constant-area method is used exclusively in the remainder of this report.

Effect of injection Mach number.- Figure 3 indicates that at a test-section Mach number of 3 $M_J = 1$ is optimum for starting, but a somewhat greater value is desirable for running. The downstream contraction used for the running condition is the maximum permissible for starting based on M_3 (subsonic), that is, $M_4 = 1$ for the starting case. The selection of $M_4 = 1$ places all running solutions on a comparable basis. If no downstream contraction is used, the running results are identical with the starting data shown. Figure 4 shows the variation of $M_{J_{opt}}$ with M_0 for the running condition with maximum downstream contraction for starting.

Effect of upstream contraction.- The results in figure 5 show the advantages of upstream contraction with and without downstream contraction for $M_0 = 3.0$, $M_J = 1.5$, and $K = 1.0$. These results also can be interpreted as meaning that, for starting ($A_1/A_2 = 1.39$ for $M_0 = 3$), $M_2 = 1$ yields the lowest compression ratios. The obvious favorable effect of downstream contraction for the running condition is also apparent in this case as it was for M_J as a primary parameter, but the magnitudes of this effect decrease as the upstream contraction increases.

One factor not considered in the above analysis is the possibility of the injector stream choking the main stream for the starting condition. This can occur for $p_J > p_2$ just downstream of the injection point, but before a significant amount of mixing has occurred. If the main stream is assumed to be choked when starting, equation (A17) of Appendix A can be derived which gives the maximum contraction ratio as a function of M_0, m, K, and M_J. M_J'' is determined by equation (A18). It is apparent that equation (A17) is invalid for $M_J'' < M_J$; that is, $p_J < p_2$. Also, it is known that, if $M_2 = 1$, p_J must be equal to or less than p_2. If $p_J = p_2$, M_J'' must equal M_J and equation (A18) determines the lowest permissible M_J for starting when $M_2 = 1$. As a result of equations (A17) and (A18), there is a starting limit corresponding to figures 5(a) and 5(b).

Effect of stagnation pressure ratio.- In figure 6 is shown the effect of K on the compression ratio of figure 5(b) ($A_1/A_2 = 1.39$) for two values of mass ratio. Since $m = K(A_J^*/A_0^*)$ (eq. (A3)), it is seen that the diffuser geometry must change in order to maintain constant m with varying K. If the geometry is fixed, the effect of K will be as shown by the curve termed "constant geometry" in figure 6. For this particular curve the abscissa of the plot also indicates mass ratio.

Effect of auxiliary injection on power requirements.- By use of equation (C3) or (C5) at $K = 1$ the theoretical power required by an auxiliary-injector wind tunnel can be compared to test-section normal-shock power, as shown in figure 7(a). This curve corresponds to the

lowest running curve of figure 5(b). Figure 7(a) shows that the lowest power occurs at $m = 0$, corresponding to an ideal fixed-geometry second throat, and, therefore, compression-ratio reduction is obtained at the expense of power.

The effect of K on power is dependent upon the method of obtaining the injector air. Two methods are shown by A and B of figure 7(b) for continuous-operation wind tunnels. The A system would be the only satisfactory way of solving the surge problem briefly discussed in the introduction. The power ratios for the two arrangements are also shown in figure 7(b), corresponding to equations (C3) and (C5). The auxiliary compressors represent throttle valves when the slopes of the curves are negative. It is apparent that $K = 1$ is optimum for minimum power of method A, but method B has a minimum corresponding to $r_J = 1$, that is, $p_{t_J} = p_{t_5}$ (fig. 1). Method B, obviously, is the least practical for mass ratios in the region of 1 because it requires an auxiliary compressor of the same magnitude as the main drive. In addition, values of $K < 1$ can have a detrimental effect on the wind-tunnel boundary layer which is not accounted for in the simple theory.

APPARATUS

The Ames 1- by 3-Foot Supersonic Tunnel No. 2

This test facility is an intermittent-type wind tunnel which utilizes compressed air from the adjacent Ames 12-foot pressure tunnel, as indicated in figure 8(a). The geometry of its flexible nozzle cannot be altered rapidly enough to permit low Mach number starting (or stopping) and high Mach number testing. The auxiliary-injector configuration selected for the 1- by 3-foot tunnel was largely determined by the existent design, and alterations were held to a minimum. The installation is indicated in figure 8(b).

The Ames 8- by 8-Inch Test Facility

This wind tunnel is a nonreturn continuous-operation type which uses the compressors of the Ames 12-foot pressure tunnel. The nozzle is of the symmetrical fixed-block type.

In figure 9(a) are shown the various diffuser profiles tested in conjunction with the $M_o \approx 3.33$ nozzle blocks (8- by 6.3-inch test section). Figure 9(b) shows the diffuser shape used with the $M_o = 3.5$ and $M_o = 3.0$ nozzle blocks (8- by 7.3-inch test section). The altered cross section of the flap in figure 9(b) represents a shape necessary

for adequate strength when the flap is fabricated for use in a large wind tunnel. Figure 10 is a photograph of the nozzle and flap arrangement corresponding to figure 9(a).

TEST MEASUREMENTS

All tests consisted of the determination of starting and stopping compression ratios. The pressure measurements were made by means of static orifices in the nozzle and injector settling chambers, and by reference to atmospheric pressure in the case of the 1- by 3-foot tunnel and to a static orifice in the end of the subsonic diffuser of the 8- by 8-inch test facility. Mass ratios were obtained from the relation $m = K (A_J^*/A_O^*)$. Such a calculation is not exact, of course, because of the different relative boundary-layer displacement thicknesses at the throats of the injector and tunnel nozzles and dissimilar subsonic entries.

COMPARISON OF THEORETICAL AND EXPERIMENTAL RESULTS

In figure 11, the test data obtained from the 1- by 3-foot blowdown tunnel are shown and compared to calculations made in accordance with the one-dimensional analysis. The mixing region was assumed to have constant cross-sectional area. Figure 12 shows the test data from the 8- by 8-inch test facility compared to similar calculations. Sample computations for both tunnels are given in Appendix D. In all cases M_J was obtained directly from the actual injector geometry, but the actual geometric values of A_1/A_2 and A_3/A_4 (8- by 8-inch test facility only) were reduced by the test-section boundary-layer displacement thickness to conform with the nonviscous (solid) boundary of figure 1. In figure 12(b) no data are shown for the original downstream contraction or modification 1 of figure 9(a) ($A_3/A_4 = 1.23$ and 1.15, respectively), because the flow choked at the minimum area for $m = 1.8$, which prevented the establishment of supersonic flow in the test section.

In figure 13 the resultant improvement in operating characteristics of the 1- by 3-foot blowdown tunnel is shown. Corresponding measurements of starting and stopping loads on a small triangular wing indicated load reductions at least in proportion to the reduction in compression ratio between the injector-off and -on conditions. The starting time also is lowered in proportion to the compression ratio which may have affected these results. However, limited tests in which the starting time was reduced from approximately 9 to 4 seconds at a fixed compression ratio did not change the peak loadings on the models. The extension of the injector curves below $M = 2.87$ is a result of more recent tests at $M = 2$ not presented in this report.

It is to be noted that both figures 11 and 12 indicate generally steeper slopes than shown in figure 5. This is believed to be an effect of the variable flap which produces greater upstream contraction with increasing m.

Figures 14(a) and 14(b) show the effect of auxiliary injection on total power requirements for the 1- by 3-foot tunnel and 8- by 8-inch test facility. The theoretical curves are based on normal-shock compression ratios and the experimental curves on compression ratios for actual wind tunnels without second throats.

The experimental tests of auxiliary air injectors indicated the following general results aside from the data previously presented:

1. The starting and stopping process of a wind tunnel with auxiliary injection is characterized by a sudden transfer of the terminal shock system from the test section to a position downstream of the injection point, similar to the action of a mechanical second throat.

2. Air injection appears to maintain attached boundary-layer flow downstream of the injection point, as compared to separated flow without injection. Figure 15 shows some schlieren pictures taken in the 1/12-scale model of the Ames 1- by 3-foot supersonic wind tunnel no. 2. Figures 15(a) and 15(b) show the large-scale separation associated with the original tunnel configuration. Both pictures represent the same compression ratio, but the unsteady nature of the flow caused fluctuations in the separation point. Typical flow patterns with air injection are shown in figures 15(c) and 15(d) which demonstrate complete flow attachment in the supersonic regions.

3. Although no tests were made specifically to determine $M_{J_{opt}}$ experimentally, available test data indicate that M_J should be above 1 and increase with M_o, with or without downstream contraction. Specifically, values of M_J about 10 percent (or more) above the M_J curve, determined by equation (A18) for $K = 1$, resulted in satisfactory operation, but values below resulted either in unsteady flow or the inability to establish supersonic flow in the range of $M_o = 2.8$ to 3.5.

DISCUSSION

The principle of operation of an auxiliary air injector, neglecting the more obvious effects of upstream and downstream contraction, appears to be as follows: For the upstream shock position (starting condition) the total pressure lost in the tunnel channel due to the shock wave and wall friction is partially returned by the injected air by means of the mixing process, provided the proper values of M_J and K are selected.

This partial return of total pressure to the main stream is equivalent to a pressure recovery and, hence, a reduction in starting compression ratio. In the case of the downstream shock location (running condition), the presence of the injector stream at a static pressure $p_J > p_2$ produces a mixing process in which the inherent losses are more than compensated by the lower total-pressure drop across the terminal normal-shock system ($M_3 < M_0$). This effect can be interpreted as meaning that the injector stream effectively contracts the tunnel flow in the manner of an "aerodynamic throat," as an analogy to mechanical second throats.

When upstream divergence ($A_1/A_2 < 1$, fig. 1) rather than upstream contraction is considered, theory predicts the lowest compression ratio for the upstream normal-shock position, as shown in figure 11 ($A_2 = A_1$ where curves cross). For this wind tunnel the normal shock can stand either at the end of the test section (lowest starting curve) or just in front of the flaps (highest starting curve), because of the diverging walls which result from the balance compensation, as shown in figure 8. With flap divergence, therefore, the upstream shock position should be termed the "running" condition, and the downstream shock position may actually never be attained in the starting process.

In figure 12(a) it is seen that M_J equaled approximately 2.4 for an M_0 of both 3.0 and 3.5 (design condition). Had M_J been lower for $M_0 = 3.0$, the compression ratios would be expected to be less than those shown.

It has been shown by figure 7(a) that, theoretically, compression-ratio reduction is obtained at the expense of the power put into the injector jet. Upstream and downstream contractions help to reduce the amount of injector flow required to attain a given compression ratio, as shown by figure 5. In figure 14 are shown theoretical and experimental power ratios for the 1- by 3-foot and 8- by 8-inch wind tunnels. Figure 14 shows generally higher theoretical power ratios than figure 7(a) which serves to indicate that lower upstream and downstream contraction ratios were used in the two auxiliary-injector designs than is theoretically possible. The experimental power ratios of figure 14 indicate power requirements for these auxiliary-injector designs up to 60 percent greater than conventional wind tunnels with divergent diffusers, and up to about 160 percent greater than a fixed second throat (ref. 7). Only the 1- by 3-foot wind-tunnel data at $M = 2.87$ and mass ratios less than 0.2 indicate power ratios of the magnitude of a fixed second-throat diffuser. In light of past knowledge, this result which warrants further investigation can be attributed to the energizing of the boundary layer. Unfortunately, test data at mass ratios less than 0.4 are not available for the other configurations to corroborate this effect.

From the foregoing power discussion it is apparent that an auxiliary injector presents no advantage from the standpoint of power consumption (except possibly for boundary-layer control) and, therefore, should not be used unless other aspects of a wind-tunnel design overshadow the power considerations. For a continuous-operation wind tunnel, auxiliary injection can be used to advantage when either the test-section nozzle cannot be varied during tunnel operation to permit low Mach number starting and high Mach number running of a mechanical second throat and/or an increase in Mach number beyond a certain point will surge the compressor system. The value of an auxiliary injector, in this case, results from the reduction in both starting and running compression ratios from those of a conventional divergent-diffuser wind tunnel, and from the fact that these compression-ratio reductions are accomplished by utilization of the excess air that otherwise would induce compressor surge. An example of such an auxiliary-injector application is given at the end of this section.

For the atmospheric-discharge intermittent-operation wind tunnel, auxiliary injection has its best application, again, only when the test-section nozzle cannot be varied rapidly during tunnel operation to permit low Mach number starting of a mechanical second throat. The advantages of reduced starting compression ratios for intermittent-operation wind tunnels have previously been covered in the section on experimental results.

In the analysis section it was concluded that the best method of predicting the performance of new designs lies in the use of empirical relations between theory and available experimental data. The simplest of such correction factors is the ratio of experimental-to-theoretical compression ratio (r_f). In figure 16, r_f has been plotted as a function of mass ratio for the 8- by 8-inch test facility and the 1- by 3-foot wind tunnel, as computed directly from figures 11 and 12.

The correction factors of figure 16 can be compared with similar values from conventional wind tunnels with divergent diffusers in order to better understand the magnitudes of r_f. In figure 17 is shown an average of the minimum compression ratios from several wind tunnels with subsonic diffusers, and a curve of normal-shock compression ratios, which is a result of the use of one-dimensional flow equations, as is the injector theory. The experimental data were obtained from references 8, 9, and 10, and figure 13. By division of this average experimental curve by the normal-shock values, the r_f curve is obtained which represents correction factors for these conventional wind tunnels. An average of the r_f curve is indicated in figure 16 for the Mach number range of 2.2 to 3.5, which are the extreme limits of M_4 as calculated according to Appendix D for the 1- by 3-foot tunnel and the 8- by 8-inch test-facility configurations.

It is apparent from figure 16 that all injector-test results, except the 1- by 3-foot tunnel data at $M = 3.35$, more closely approach one-dimensional predictions than do the conventional wind tunnels. A possible reason for this may be indicated by figure 15 for which it has previously been pointed out that a subsonic diffuser without air injection (boundary-layer control) experiences large-scale separation; whereas air injection reduces the degree of separation. Since the theory assumes attached flow, it would be expected that a one-dimensional analysis would be a better approximation for auxiliary-injector tunnels than for conventional subsonic-diffuser tunnels.

A comparison of the correction factors in figure 16 for the two wind tunnels indicates the 8- by 8-inch test-facility diffuser design to be preferable, primarily, because of the high r_f values for the 1- by 3-foot tunnel data at $M = 3.35$.

On the basis of an empirical curve faired through the r_f values in figure 16 and one-dimensional-injector analysis, it is possible to predict the performance of other designs. In Appendix E, a recommended procedure is given for this purpose, together with additional considerations based on experimental results.

A typical application of the auxiliary-injector principle to a wind-tunnel design of the closed-circuit, continuous-operation type can be demonstrated by use of a compressor performance curve similar to that of figure 5.17 of reference 8. In figure 18(a) this is shown as compressor no. 1, together with the average compression-ratio required curve of figure 17. The diagonal lines are curves of constant Mach number (throttle curves) for a 1-square-foot tunnel and $T_{t_o} = 570^\circ$ Rankine.

For this wind-tunnel design, the maximum possible test-section Mach number is under 2.5. If the test results of reference 11 are used to estimate the performance of a variable-geometry second throat, the r required for starting and running will be approximately as shown in figure 18(a). These tests included a cone model and circular-arc support system which more closely approximates the experimental results of this report. The starting compression ratio for a partially contracted second throat, as compared to the data of figure 17, is apparently much lower. This improvement is possibly attributable, in part, to the lack of flow separation which usually results from the use of a divergent diffuser immediately following the test section. By use of the variable-geometry second-throat requirements shown in the figure, a smaller compressor can be selected (compressor no. 2, fig. 18(a)). For this case it is seen that the maximum Mach number is limited to about 2.9 by the surge limit of the compressor and the starting compression ratio, if a test-section nozzle capable of varying Mach number during operation is not available. By reducing compressor speed to approach more closely

the required curves for the running condition, a power saving can be achieved contingent upon the method of speed control and the variation of compressor efficiency with speed. By use of the original compressor size (no. 1), the auxiliary injector presents the possibility of attaining Mach numbers above 2.9 by overspeeding the compressor for starting. (For the second-throat example, overspeeding to start above a Mach number of 3 appears impractical because of the steepness of the compression-ratio required curve.) As an example of the amount of air available for bypassing to the injectors, at a given operating point C, the quantity of air entering the injectors at $M = 2.9$ is BC and that passing through the test section is AB, or a mass ratio of 0.63.

If the design procedure of Appendix E is followed, an auxiliary-injector performance curve can be calculated as shown in figure 18(b). The design point is $M = 2.90$ and bypassing begins at $M = 2.40$. If above $M = 2.90$ the diffuser wall is made adjustable in the region of the injector flap, in order to obtain the required M_J and A_1/A_2 values, the r required curves up to $M = 3.50$ can be obtained.

This example of the use of auxiliary injection for continuous-operation wind tunnels indicates that its best application is for extending the speed range of existing wind tunnels where the compressor has been selected on the basis of the compression ratio required by a divergent diffuser.

CONCLUSIONS

From the analytic and experimental results presented in this report of the application of air injectors to supersonic wind tunnels, the following conclusions can be drawn:

1. In general, an auxiliary air-injector system can reduce both starting and running compression ratios, as compared to a conventional wind tunnel with a divergent diffuser.

2. This compression-ratio reduction entails an increase in power requirements, except at mass ratios less than about 0.2. A limited amount of data in this range shows promise of reducing power requirements through boundary-layer control.

3. An auxiliary air-injector system applied to a continuous-operation wind tunnel of variable Mach number and conventional compressor drive unit can extend the Mach number range without surging the compressor and can reduce starting difficulties. These results are obtainable without additional pumping equipment.

4. The auxiliary injector system, from the standpoint of continuous-operation tunnels, is basically not a power-saving device, but, rather, an artifice through which the restricted characteristics of conventional air compressors can be more closely alined with supersonic-wind-tunnel requirements.

5. An auxiliary air-injector system applied to a blowdown-type wind tunnel with a divergent diffuser can reduce starting loads, increase running time, and raise the maximum operating Mach number.

6. Although all parameters involved in this injector application are not fully evaluated experimentally, sufficient information is presented to predict the performance of future designs which do not differ radically from the experimental configurations described herein.

Ames Aeronautical Laboratory
National Advisory Committee for Aeronautics
Moffett Field, Calif., Sept. 1, 1953

APPENDIX A

DERIVATION OF AUXILIARY-INJECTOR EQUATIONS FOR CONSTANT-AREA CASE

$$(A_3 = A_J + A_2)$$

For the adiabatic flow of a perfect gas the energy equation can be written between stations c and d of figure 1 as follows:

$$\rho_2 A_2 V_2 C_p T_{t_2} + \rho_J A_J V_J C_p T_{t_J} = \rho_3 A_3 V_3 C_p T_{t_3}$$

It can be simply shown that, when $T_{t_2} = T_{t_J}$, the energy equation reduces to

$$T_{t_3} = T_{t_2} = T_{t_J} \tag{A1}$$

and therefore a^* is constant throughout the flow. The continuity equation can be written as

$$\rho_o^* A_o^* a^* + \rho_J^* A_J^* a^* = \rho_3 A_3 V_3$$

Dividing by ρ_o^*, A_o^*, and a^*

$$1 + m = \frac{\rho_3}{\rho_o^*} \frac{A_3}{A_o^*} \frac{V_3}{a^*} \tag{A2}$$

where

$$m = \frac{\rho_J^* A_J^* a_J^*}{\rho_o^* A_o^* a^*} = K \frac{A_J^*}{A_o^*} = K\left(\frac{A^*}{A}\right)_J \qquad \frac{A_J}{A_o^*} = K \frac{\left(\frac{A^*}{A}\right)_J}{\left(\frac{A^*}{A}\right)_o} \frac{A_J}{A_o} \tag{A3}$$

$$\frac{\rho_3}{\rho_o^*} = \frac{\frac{\rho_3}{\rho_{t_3}} \rho_{t_3}}{\frac{\rho_o^*}{\rho_{t_o}} \rho_{t_o}} = \frac{\left(\frac{\rho}{\rho_t}\right)_3}{\left(\frac{\rho}{\rho_t}\right)^*} \frac{p_{t_3}}{p_{t_o}} \tag{A4}$$

$$\frac{V_s}{a^*} = M_s \frac{\left(\frac{a}{a_t}\right)_s}{\left(\frac{a}{a_t}\right)^*} \tag{A5}$$

and

$$\left(\frac{A^*}{A}\right) = M\left(\frac{\frac{\gamma+1}{2}}{1+\frac{\gamma-1}{2}M^2}\right)^{\frac{\gamma+1}{2(\gamma-1)}}$$

$$\left(\frac{\rho}{\rho_t}\right) = \left(1+\frac{\gamma-1}{2}M^2\right)^{-\frac{1}{\gamma-1}}$$

$$\left(\frac{T}{T_t}\right) = \left(1+\frac{\gamma-1}{2}M^2\right)^{-1}$$

$$\left(\frac{a}{a_t}\right) = \left(\frac{T}{T_t}\right)^{1/2}$$

Also,

$$\frac{A_s}{A_o{}^*} = \frac{A_2 + A_J}{\left(\frac{A^*}{A}\right)_o A_o} = \frac{1}{\left(\frac{A^*}{A}\right)_o}\left(\frac{A_2}{A_1}+\frac{A_J}{A_o}\right) = \frac{1}{\left(\frac{A^*}{A}\right)_o}\left[\frac{A_2}{A_1}+\frac{m}{K}\frac{\left(\frac{A^*}{A}\right)_o}{\left(\frac{A^*}{A}\right)_J}\right] \tag{A6}$$

When equations (A4) and (A5) are substituted into equation (A2), the mixing-loss compression ratio is found to be

$$r_m = \frac{p_{t_o}}{p_{t_s}} = \frac{\left(\frac{\rho}{\rho_t}\right)_s \left(\frac{a}{a_t}\right)_s M_s}{\left(\frac{\rho}{\rho_t}\right)^* \left(\frac{a}{a_t}\right)^*} \frac{\frac{A_s}{A_o{}^*}}{(1+m)} = \left(\frac{A^*}{A}\right)_s \frac{\frac{A_s}{A_o{}^*}}{(1+m)}$$

If equation (A6) is used

$$r_m = \frac{\left(\frac{A^*}{A}\right)_3 \frac{A_3}{A_0^*}}{1+m} = \frac{\left(\frac{A^*}{A}\right)_3}{\left(\frac{A^*}{A}\right)_0}\left[\frac{\frac{A_2}{A_1} + \frac{m}{K}\frac{(A^*/A)_0}{(A^*/A)_J}}{(1+m)}\right] \tag{A7}$$

The total momentum equation for any mixing-tube shape is

$$A_2(\rho_2 V_2^2 + p_2) + A_J(\rho_J V_J^2 + p_J) + \int_{A_2+A_J}^{A_3} p_w\left(\frac{dA}{dx}\right)dx = A_3(\rho_3 V_3^2 + p_3) \tag{A8}$$

Since $A_3 = A_2 + A_J$, the integral term is zero. Hence,

$$A_2(\rho_2 V_2^2 + p_2) + A_J(\rho_J V_J^2 + p_J) = A_3(\rho_3 V_3^2 + p_3)$$

Since $\rho = p/RT$ and $V^2 = M^2\gamma RT$ the momentum equation can be written as

$$p_2 A_2(\gamma M_2^2 + 1) + p_J A_J(\gamma M_J^2 + 1) = p_3 A_3(\gamma M_3^2 + 1)$$

dividing by p_{t_0} and A_0

$$\left(\frac{p}{p_t}\right)_2 \frac{p_{t_2}}{p_{t_0}} \frac{A_2}{A_0}(\gamma M_2^2 + 1) + \left(\frac{p}{p_t}\right)_J K \frac{A_J}{A_0}(\gamma M_J^2 + 1) = \left(\frac{p}{p_t}\right)_3 \frac{p_{t_3}}{p_{t_0}} \frac{A_3}{A_0}(\gamma M_3^2 + 1)$$

where

$$\left(\frac{p}{p_t}\right) = \left(1 + \frac{\gamma-1}{2} M^2\right)^{-\frac{\gamma}{\gamma-1}}$$

When equations (A3) and (A6) are used, the momentum equation becomes

$$\left(\frac{p}{p_t}\right)_2 \left(\frac{p_t'}{p_t}\right)_0 \frac{A_2}{A_1}(\gamma M_2^2 + 1) + \left(\frac{p}{p_t}\right)_J m \frac{\left(\frac{A^*}{A}\right)_0}{\left(\frac{A^*}{A}\right)_J}(\gamma M_J^2 + 1) = \frac{\left(\frac{p}{p_t}\right)_3}{\left(\frac{p_{t_0}}{p_{t_3}}\right)}\left[\frac{A_2}{A_1} + \frac{m}{K}\frac{\left(\frac{A^*}{A}\right)_0}{\left(\frac{A^*}{A}\right)_J}\right](\gamma M_3^2 + 1) \tag{A9}$$

where

$$\left(\frac{p_t'}{p_t}\right)=\left[\frac{(\gamma+1)M^2}{(\gamma-1)M^2+2}\right]^{\frac{\gamma}{\gamma-1}}\left[\frac{2\gamma M^2-(\gamma-1)}{\gamma+1}\right]^{-\frac{1}{\gamma-1}}$$

Equations (A7) and (A9) are two equations in two unknowns (M_3 and $p_{t_0}/p_{t_3} = r_m$). When equation (A7) is substituted into the right-hand side of (A9), a function of M_3 can be obtained

$$f(M_3) = \frac{\left(\frac{p}{p_t}\right)_3 (\gamma M_3^2 + 1)}{\left(\frac{A^*}{A}\right)_3} =$$

$$\frac{\left(\frac{p_t'}{p_t}\right)_0\left(\frac{p}{p_t}\right)_2 \frac{A_2}{A_1}(\gamma M_2^2 + 1)}{\left(\frac{A^*}{A}\right)_0 (1+m)} + m\frac{\left(\frac{p}{p_t}\right)_J (\gamma M_J^2 + 1)}{\left(\frac{A^*}{A}\right)_J (1+m)}$$

Since $\left(\frac{A^*}{A}\right)_0 = \frac{A_1^*}{A_2}\frac{A_0^*}{A_1^*}\frac{A_2}{A_1} = \left(\frac{A^*}{A}\right)_2\left(\frac{p_t'}{p_t}\right)_0\frac{A_2}{A_1}$,

$$\left[\frac{\left(\frac{p}{p_t}\right)_3 (\gamma M_3^2 + 1)}{\left(\frac{A^*}{A}\right)_3}\right] = \frac{1}{1+m}\left\{\left[\frac{\left(\frac{p}{p_t}\right)_2 (\gamma M_2^2 + 1)}{\left(\frac{A^*}{A}\right)_2}\right] + m\left[\frac{\left(\frac{p}{p_t}\right)_J (\gamma M_J^2 + 1)}{\left(\frac{A^*}{A}\right)_J}\right]\right\}$$

or

$$f(M_3) = \frac{1}{1+m}\left[f(M_2) + mf(M_J)\right] \qquad \text{(A10)}$$

with the requirement that $M_3 > 1$ for $M_2 > 1$ and $M_3 < 1$ for $M_2 < 1$.

All f(M) terms can be obtained from one plot of f(M) against M. For the starting and running conditions with upstream contraction, M_2 is obtained from

$$\left(\frac{A^*}{A}\right)_2 = \left(\frac{A^*}{A}\right)_1 \frac{A_1}{A_2} \tag{A11}$$

For $(A_1/A_2) < 1$, see Appendix E, step 7. For the starting condition (from normal-shock relations),

$$M_1 = \left(\frac{1 + \frac{\gamma-1}{2} M_o^2}{\gamma M_o^2 - \frac{\gamma-1}{2}}\right)^{1/2} = \frac{1}{\left(\frac{a}{a_t}\right)_o \left(\gamma M_o^2 - \frac{\gamma-1}{2}\right)^{1/2}} \tag{A12}$$

If a normal shock is assumed to terminate the flow after mixing, the compression ratio of the tunnel can be expressed as

$$r = \frac{r_m}{\left(\frac{p_t'}{p_t}\right)_3} \tag{A13}$$

If the flow is isentropically contracted from station d to e, the tunnel compression ratio is

$$r = \frac{r_m}{\left(\frac{p_t'}{p_t}\right)_4} \tag{A14}$$

For the starting condition, (p_t'/p_t) equals 1 in equations (A13) and (A14). The value M_4 is obtained from M_3 by use of the following area relations:

$$\left(\frac{A^*}{A}\right)_4 = \left(\frac{A^*}{A}\right)_3 \frac{A_3}{A_4} = \left(\frac{A^*}{A}\right)_3 \left(\frac{A_2 + A_J}{A_4}\right) = \left(\frac{A^*}{A}\right)_3 \frac{A_1}{A_4} \left(\frac{A_2}{A_1} + \frac{A_J}{A_1}\right)$$

Using equation (A3)

$$\left(\frac{A^*}{A}\right)_4 = \left(\frac{A^*}{A}\right)_3 \frac{A_3}{A_4} = \left(\frac{A^*}{A}\right)_3 \frac{A_1}{A_4} \left[\frac{A_2}{A_1} + \frac{m}{K} \frac{\left(\frac{A^*}{A}\right)_o}{\left(\frac{A^*}{A}\right)_J}\right] \tag{A15}$$

It is possible to determine a relation between the variables when the main stream is choked just downstream of the injection station. Letting superscript double prime denote the condition after equalization of pressures but before mixing begins, then

$$A_J + A_2 = A_J'' + A_2'' = A_J'' + A_2^*$$

when $M_2'' = 1$

We divide by A_2^* and note that $(A^*/A)_2 = (A^*/A)_1 A_1/A_2$, then

$$\frac{A_J}{A_2^*} + \frac{1}{\left(\frac{A^*}{A}\right)_1 \frac{A_1}{A_2}} = \frac{A_J''}{A_2^*} + 1 \tag{A16}$$

Since

$$\frac{A_J}{A_2^*} = \frac{A_J}{A_J^*}\frac{A_J^*}{A_o^*}\frac{A_o^*}{A_2^*} = \frac{m}{K\left(\frac{A^*}{A}\right)_J}\left(\frac{p_t'}{p_t}\right)_o$$

and, similarly,

$$\frac{A_J''}{A_2^*} = \frac{m}{K\left(\frac{A^*}{A}\right)_J''}\left(\frac{p_t'}{p_t}\right)_o$$

When the above two equations are substituted in equation (A16) and solved for A_1/A_2,

$$\frac{A_1}{A_2} = \frac{1}{\left(\frac{A^*}{A}\right)_1\left\{\frac{m}{K}\left(\frac{p_t'}{p_t}\right)_o\left[\frac{1}{(A^*/A)_J''} - \frac{1}{(A^*/A)_J}\right] + 1\right\}} \tag{A17}$$

Hence, A_1/A_2 is the maximum upstream contraction ratio that permits starting, $(A^*/A)_J''$ is determined by (for $p_J'' = p_2''$).

$$\left(\frac{p}{p_t}\right)_J'' = \frac{p_2''}{p_{t_2}}\frac{p_{t_2}}{p_{t_o}}\frac{p_{t_o}}{p_{t_J}} = \frac{0.5283}{K}\left(\frac{p_t'}{p_t}\right)_o \tag{A18}$$

APPENDIX B

DERIVATION OF AUXILIARY-INJECTOR EQUATIONS FOR CONSTANT-PRESSURE CASE

$$(p_w = p_J = p_3)$$

Since $A_3 \neq A_J + A_2$, the continuity equation (A7) is

$$r_m = \frac{\left(\frac{A^*}{A}\right)_3}{(1+m)} \frac{A_3}{A_0^*} = \frac{p_{t_0}}{p_{t_3}} = \frac{p_{t_0}}{\frac{p_{t_3}}{p_3} p_J} = \frac{\left(\frac{p}{p_t}\right)_3}{\left(\frac{p}{p_t}\right)_J K} \tag{B1}$$

or

$$\frac{A_3}{A_0^*} = \frac{\left(\frac{p}{p_t}\right)_3}{K\left(\frac{p}{p_t}\right)_J} \frac{(1+m)}{\left(\frac{A^*}{A}\right)_3} \tag{B2}$$

$$\frac{A_3}{A_2} = \frac{A_3}{A_0^*} \left(\frac{A^*}{A}\right)_0 \frac{A_1}{A_2} = \frac{1}{K} \frac{\left(\frac{p}{p_t}\right)_3 \left(\frac{A^*}{A}\right)_0}{\left(\frac{p}{p_t}\right)_J \left(\frac{A^*}{A}\right)_3} \frac{A_1}{A_2} (1+m) \tag{B3}$$

Since $p_w = p_J = p_3$, the momentum equation can be written from (A8) as

$$A_2(\rho_2 V_2^2 + p_2) + A_J(\rho_J V_J^2 + p_J) + p_J(A_3 - A_2 - A_J) = A_3(\rho_3 V_3^2 + p_J)$$

or

$$A_2(\rho_2 V_2^2 + p_2) + \rho_J A_J V_J^2 - p_J A_2 = \rho_3 A_3 V_3^2$$

Since $\rho = \frac{p}{RT}$ and $V^2 = M^2 \gamma RT$,

$$p_2 A_2(\gamma M_2^2 + 1) + p_J A_2\left(\gamma \frac{A_J}{A_2} M_J^2 - 1\right) = \gamma p_J A_3 M_3^2$$

We divide by p_{t_o} and A_2

$$\left(\frac{p}{p_t}\right)_2 \left(\frac{p_t'}{p_t}\right)_o (\gamma M_2^2+1) + \left(\frac{p}{p_t}\right)_J K\left(\gamma \frac{A_J}{A_2} M_J^2 - 1\right) = \gamma K \left(\frac{p}{p_t}\right)_J \frac{A_3}{A_2} M_3^2 \tag{B4}$$

where $(p_t'/p_t) = 1$ for $M_2 > 1$; substitute equation (B3) in (B4) and solve for $f(M_3)$

$$\left(\frac{p}{p_t}\right)_3 \frac{M_3^2}{\left(\frac{A^*}{A}\right)_3} = \frac{1}{\gamma\left(\frac{A^*}{A}\right)_o \frac{A_1}{A_2}(1+m)} \left[\left(\frac{p}{p_t}\right)_2 \left(\frac{p_t'}{p_t}\right)_o (\gamma M_2^2 + 1) + K\left(\frac{p}{p_t}\right)_J \left(\gamma \frac{A_J}{A_2} M_J^2 - 1\right)\right]$$

or, noting that $\left(\frac{A^*}{A}\right) = M \frac{\left(\frac{p}{p_t}\right)\left(\frac{a}{a_t}\right)^*}{\left(\frac{p}{p_t}\right)^*\left(\frac{a}{a_t}\right)}$,

$$f(M_3) = \left(\frac{a}{a_t}\right)_3 M_3 = \frac{\left(\frac{a}{a_t}\right)_o \left[\left(\frac{p}{p_t}\right)_2 \left(\frac{p_t'}{p_t}\right)_o (\gamma M_2^2 + 1) + K\left(\frac{p}{p_t}\right)_J \left(\gamma \frac{A_J}{A_2} M_J^2 - 1\right)\right]}{\gamma M_o \left(\frac{p}{p_t}\right)_o \frac{A_1}{A_2}(1+m)} \tag{B5}$$

If A_J/A_2 is not known, it may be obtained from equation (A3)

$$\frac{A_J}{A_2} = \frac{m}{K} \frac{A_1}{A_2} \frac{\left(\frac{A^*}{A}\right)_o}{\left(\frac{A^*}{A}\right)_J} \tag{B6}$$

The resultant contraction ratio is from (B3) and (B6)

$$\frac{A_2 + A_J}{A_3} = \frac{1 + \frac{A_J}{A_2}}{\frac{A_3}{A_2}} = \frac{K\left(\frac{p}{p_t}\right)_J \left(\frac{A^*}{A}\right)_3}{\left(\frac{p}{p_t}\right)_3 \left(\frac{A^*}{A}\right)_0} \frac{\left[\frac{A_2}{A_1} + \frac{m}{K} \frac{(A^*/A)_0}{(A^*/A)_J}\right]}{(1 + m)} \tag{B7}$$

APPENDIX C

EQUATIONS FOR POWER REQUIREMENTS

The power required by an auxiliary-injector wind tunnel can be compared to any conventional type (no auxiliary air injection) by use of the isentropic compression relations. As shown in figure 7(b) there are two possible ways of obtaining the injector air.

Method A

The isentropic power required by compression can be expressed as

$$P = C \frac{p_D}{r} Q \left(r^{0.286} - 1 \right) = C \frac{p_D}{r} QY \tag{C1}$$

so that the total power (P_T) required by the main-drive and injector compressors for an auxiliary-injector tunnel of type A (fig. 7(b)) is

$$P_T = C \left(\frac{p_{D_N}}{r_N} Q_T Y_N + \frac{p_{D_J}}{r_J} Q_J Y_J \right)$$

where Q_T is the flow quantity entering the main-drive compressor.

Since $r_J = K = \frac{p_{D_J}}{p_{D_N}}$ and $\frac{Q_J}{Q_T} = \frac{1}{r_N} \frac{m}{1 + m}$,

$$P_T = C \frac{p_{D_N}}{r_N} Q_T Y_N \left(1 + \frac{m}{1 + m} \frac{Y_J}{Y_N} \right) \tag{C2}$$

Flow quantity can be expressed as (ref. 8)

$$Q = C \left(\frac{A^*}{A} \right)_o A_o \, r \sqrt{T_t}$$

and

$$Q_T = Q_N + r_N Q_J = C \left(\frac{A^*}{A} \right)_o A_o r_N (1 + m) \sqrt{T_t}$$

hence, a power ratio, for equal pressures and temperatures in the settling chamber, can be written by dividing (C2) by (C1)

$$\frac{P_T}{P_c} = \frac{Y_N}{Y_c}\left[1 + m\left(1 + \frac{Y_J}{Y_N}\right)\right] \tag{C3}$$

where Y_J is determined by $r_J = K$.

Method B

For the type B arrangement, the total power required by an auxiliary-injector tunnel is

$$P_T = P_N + P_J = C\left(\frac{p_{D_N}}{r_N} Q_N Y_N + \frac{p_{D_J}}{r_J} Q_J Y_J\right) = C\,\frac{p_{D_N}}{r_N} Q_N Y_N\left(1 + m\,\frac{Y_J}{Y_N}\right) \tag{C4}$$

The power ratio, analogous to (C3), can be written by dividing (C4) by (C1) and using the definition for Q

$$\frac{P_T}{P_c} = \frac{Y_N}{Y_c}\left(1 + m\,\frac{Y_J}{Y_N}\right) \tag{C5}$$

where Y_J is determined by $r_J = Kr_N$. It is to be noted that equations (C3) and (C5) are identical when $K = 1$; that is, $Y_J/Y_N = 0$ for method A and $Y_J/Y_N = 1$ for method B.

APPENDIX D

SAMPLE CALCULATIONS

The 8- by 8-Inch Test Facility

Given the following values and the notation of figure 1:

$M_0 = 3.50$ from test-section calibration

$M_1 = 0.451$ from normal-shock relations

$m = 1.80$ (selected)

$K = 1.0$ (selected)

$M_J = 2.42$ from injector geometry at $m = 1.8$

$\frac{A_2}{A_1} = 0.925$ from injector geometry at $m = 1.8$ (including blockage of strut)

It is to be noted that in all the following calculations, the cross-sectional areas (A) of the ducts can be interpreted as heights because the width of the ducts are held constant. Because these calculations are for an existing wind tunnel, A_2/A_1 should be reduced by the displacement thickness of the boundary layer to approximate the nonviscous boundary of figure 1 (solid line). For this wind tunnel the displacement thickness for all four walls is equivalent to approximately one-half inch on the top and bottom walls. Since the test section half-height is 3.645 inches, the corrected upstream contraction is

$$\frac{A_2}{A_1} = \frac{0.925 \times 3.645 - 0.500}{3.645 - 0.500} = 0.913$$

and the corrected downstream contraction is (see the dimensions on fig. 9)

$$\frac{A_4}{A_3} = \frac{5.165 - 0.500}{5.589 - 0.500} = 0.917$$

Starting.- From equation (A11), M_2 can be determined.

$$\left(\frac{A^*}{A}\right)_2 = 0.691 \times \frac{1}{0.913} = 0.757$$

from which $M_2 = 0.510$. We use equation (2), the N column of reference 6, and note that $M_3 < 1$ for $M_2 < 1$

$$f(M_3) = \frac{1}{(1+1.8)}\left(\frac{1}{0.3835} + 1.8 \times \frac{1}{0.3876}\right) = \frac{1}{0.3860}$$

from which $M_3 = 0.517$. By application of equation (A11) to the downstream contraction, M_4 can be determined.

$$\left(\frac{A^*}{A}\right)_4 = 0.764 \times \frac{1}{0.917} = 0.833$$

from which $M_4 = 0.591$. From equation (1)

$$r = \frac{0.764}{0.147}\,\frac{\left(0.913 + \frac{1.8}{1} \times \frac{0.147}{0.411}\right)}{(1 + 1.8)} = 2.89$$

It is to be noted that M_4 for starting was not used in the determination of r, but its value serves to indicate if starting is theoretically possible ($M_4 < 1$).

Running.- By equation (A11)

$$\left(\frac{A^*}{A}\right)_2 = 0.147 \times \frac{1}{0.913} = 0.161$$

from which $M_2 = 3.40$. Equation (2) with $M_3 > 1$ for $M_2 > 1$ yields

$$f(M_3) = \frac{1}{(1+1.8)}\left(\frac{1}{0.3601} + 1.8 \times \frac{1}{0.3876}\right) = \frac{1}{0.3775}$$

from which $M_3 = 2.71$. If equation (A11) is applied to the downstream contraction

$$\left(\frac{A^*}{A}\right)_4 = 0.311 \times \frac{1}{0.917} = 0.339$$

hence, $M_4 = 2.62$. From equation (1)

$$r = \frac{0.311}{0.147}\,\frac{\left(0.913 + \frac{1.8}{1} \times \frac{0.147}{0.411}\right)}{(1 + 1.8) \times 0.453} = 2.60$$

The 1- by 3-Foot Supersonic Wind Tunnel No. 2

For this wind tunnel the running condition can be computed in the same manner as the 8- by 8-inch tunnel. However, the starting condition requires positioning of the upstream normal shock in the region of greatest area. When the flap is deflected, it is shown in figure 8 that the largest area is at the point of 1.75-inch balance compensation.

Given:

$M_o = 3.35$ (obtained from test-section calibration)

$m = 1.00$ (selected)

$K = 1.00$ (selected)

$M_J = 1.74$ from injector geometry at $m = 1$

$\frac{A_2}{A_1} = 0.955$ from injector geometry at $m = 1$ (including blockage of model support)

$\frac{A_3}{A_4} = 1.00$ (assumed)

Starting.- To use the existing equations, M_o must have the value immediately upstream of the normal-shock position. The displacement thickness for this wind tunnel for all four walls is equivalent to approximately 1-1/2 inches on the top and bottom walls of the test section. Hence, the half-height of the channel at the upstream normal-shock position is

$$A = 13.0 + 1.75 - 0.5 = 13.3$$

where 0.5 is equivalent to one-half the sting area. The geometric expansion ratio adjusted for boundary layer is

$$\frac{A}{A_1} = \frac{14.3 - 1.5}{13 - 1.5} = 1.11$$

from which an adjusted M_o can be obtained

$$\left(\frac{A^*}{A}\right)_o = 0.170 \times \frac{1}{1.11} = 0.153$$

Therefore, the adjusted $M_0 = 3.45$ and $M_1 = 0.453$; $\frac{A_2}{A_1}$ corrected for boundary layer becomes

$$\frac{A_2}{A_1} = \frac{0.955 \times 13 - 1.5}{13 - 1.5} = 0.948$$

and the adjusted contraction is

$$0.948 \times \frac{1}{1.11} = 0.854$$

By the use of equation (All) M_2 can be determined.

$$\left(\frac{A^*}{A}\right)_2 = 0.693 \times \frac{1}{0.854} = 0.811$$

from which $M_2 = 0.565$. Equation (2) and reference 6 yield

$$f(M_3) = \frac{1}{(1+1)}\left(\frac{1}{0.4028} + \frac{1}{0.4209}\right) = \frac{1}{0.4115}$$

from which $M_3 = 0.594$. From equation (1)

$$r = \frac{0.837}{0.154}\,\frac{\left(0.854 + \frac{0.154}{0.727}\right)}{(1 + 1)} = 2.90$$

Running.- The corrected contraction is 0.948, as given in the starting case. From equation (All) M_2 can be determined.

$$\left(\frac{A^*}{A}\right)_2 = 0.170 \times \frac{1}{0.948} = 0.179$$

from which $M_2 = 3.30$. By use of equation (2)

$$f(M_3) = \frac{1}{(1+1)}\left(\frac{1}{0.3621} + \frac{1}{0.4209}\right) = \frac{1}{0.3892}$$

from which $M_3 = 2.38$. From equation (1)

$$r = \frac{0.424}{0.1695} \frac{\left(0.948 + \frac{0.170}{0.727}\right)}{(1+1) \times 0.549} = 2.68$$

APPENDIX E

DESIGN PROCEDURE

The effects of all auxiliary-injector parameters have not been established experimentally. However, on the basis of the one-dimensional analysis and existing experimental data, the following design procedure and recommendations are presented:

1. In figure 1 the solid outline of the wind tunnel can be assumed to represent nonviscous air flow for a given Mach number, and the final wall shape will be shifted by the displacement thickness as indicated by the dotted lines. Either form of equation (A7) can be used to obtain r_m after M_3 has been calculated. The first, or simpler form is useful when a scale layout of the injector installation has been made, from which A_3 can be measured. The second form requires no layout because it includes the geometric equivalent of A_3/A_0^*. In the latter case A_2/A_1 should be determined for the nonviscous boundary.

2. Select upstream contraction for the design condition to be not more than 94 percent of the theoretical value, that is,

$$\frac{A_1}{A_2} = \frac{0.94}{\left(\frac{A^*}{A}\right)_1}$$

The constant is obtained from available experimental data. A maximum wedge angle of 5° is recommended at the design condition.

3. Select M_J to be about 10 percent above the Mach number determined by

$$\left(\frac{p}{p_t}\right)_J = 0.5283 \left(\frac{p_t'}{p_t}\right)_0$$

4. The use of hinged flaps (see figs. 8 and 9) and a fixed diffuser wall is recommended when possible because of its simplicity and ability to increase A_1/A_2 and M_J with increasing m. Design the flap based on item 2 and structural requirements, and lay out an injector nozzle at the design M_J and A_J^* by area ratio $\left(A_J^* = \frac{m}{K} A_0^*\right)$. A value of K close to unity, theoretically, gives the lowest compression for a fixed mass ratio and upstream contraction, but values of K as low as 0.5 have indicated no difficulties in actual operation.

5. The need for downstream contraction when the tunnel is to be started and run at the same Mach number is not fully determined. Theoretically, downstream contraction does not improve the starting compression ratio but, experimentally, it does (fig. 12, $M_0 = 3.33$). The downstream contraction ratio in this case is 1.085.

6. Avoid any wall divergence downstream of the injection point for at least two tunnel heights.

7. By use of equations (A7) and (A10) to (A15), and the faired r_f curve (fig. 16), calculate the theoretical performance of the proposed design for the range of mass ratios under consideration. For the starting condition, the normal shock must be assumed to stand in the region of greatest area for $A_1/A_2 > 1$. When $A_1/A_2 < 1$, at a low mass ratio, for example, the downstream position can be considered as the starting condition and the upstream shock position as the running condition as previously discussed.

8. Before proceeding to the drafting stage of the design, increase the nozzle and test-section dimensions by the estimated displacement thickness. Downstream of the end of the test section a constant correction equal to that at the end of the test section is satisfactory.

9. It is recommended that model tests be made when an injector installation is intended for a large wind tunnel. This is desirable because of the uncertainty of the amount of upstream and downstream contraction that can be utilized without choking the flow.

REFERENCES

1. Rayle, R. E.: Starting Supersonic Wind Tunnels by Pressure Waves. MIT Term Project No. 39, May 1949.

2. Bradfield, Walter S.: Experimental Study of the Application of Pressure Transients to the Starting of a Supersonic Wind Tunnel. University of Minnesota, Rep. 70, Oct. 1950 (limited availability).

3. Yen, S. M., Armstrong, Gene L., and McCloy, R. W.: Mixing, Diffusion, and Pressure Recovery in the Ejector Jet. Institute of Aeronautics, University of Illinois, Rep. 9-6, 1949.

4. Bidwell, Jerold Morse: Analysis of an Induction Blowdown Supersonic Tunnel. NACA TN 2040, 1950.

5. Keenan, J. H., Neumann, E. P., and Lustwerk, F.: An Investigation of Ejector Design by Analysis and Experiment. Jour. Appl. Mech., vol. 17, no. 3, Sept. 1950, pp. 299-309.

6. Foa, Joseph V.: Mach Number Functions for Ideal Diatomic Gases. Cornell Aeronautical Lab., Inc., Oct. 1949.

7. Neumann, Ernest P., and Lustwerk, F.: High-Efficiency Supersonic Diffusers. MIT Meteor Rep. No. 56, June 1950.

8. Liepmann, Hans Wolfgang, and Puckett, Allen E.: Introduction to Aerodynamics of a Compressible Fluid. John Wiley and Sons, Inc., 1947, p. 86.

9. Wegener, P.: On the Experimental Investigation of Hypersonic Flow. Naval Ordnance Lab. Memo. 9629, July 29, 1948.

10. Eggink, Dr. H.: The Improvement in Pressure Recovery in Supersonic Wind Tunnels. R.A.E. Rep. No. Aero. 2326, S.D. 34, May 1949.

11. Diggins, J. L., and Lange, A. H.: A Systematic Study of a Variable Area Diffuser for Supersonic Wind Tunnels. NAVORD Rep. 2421, Dec. 1952.

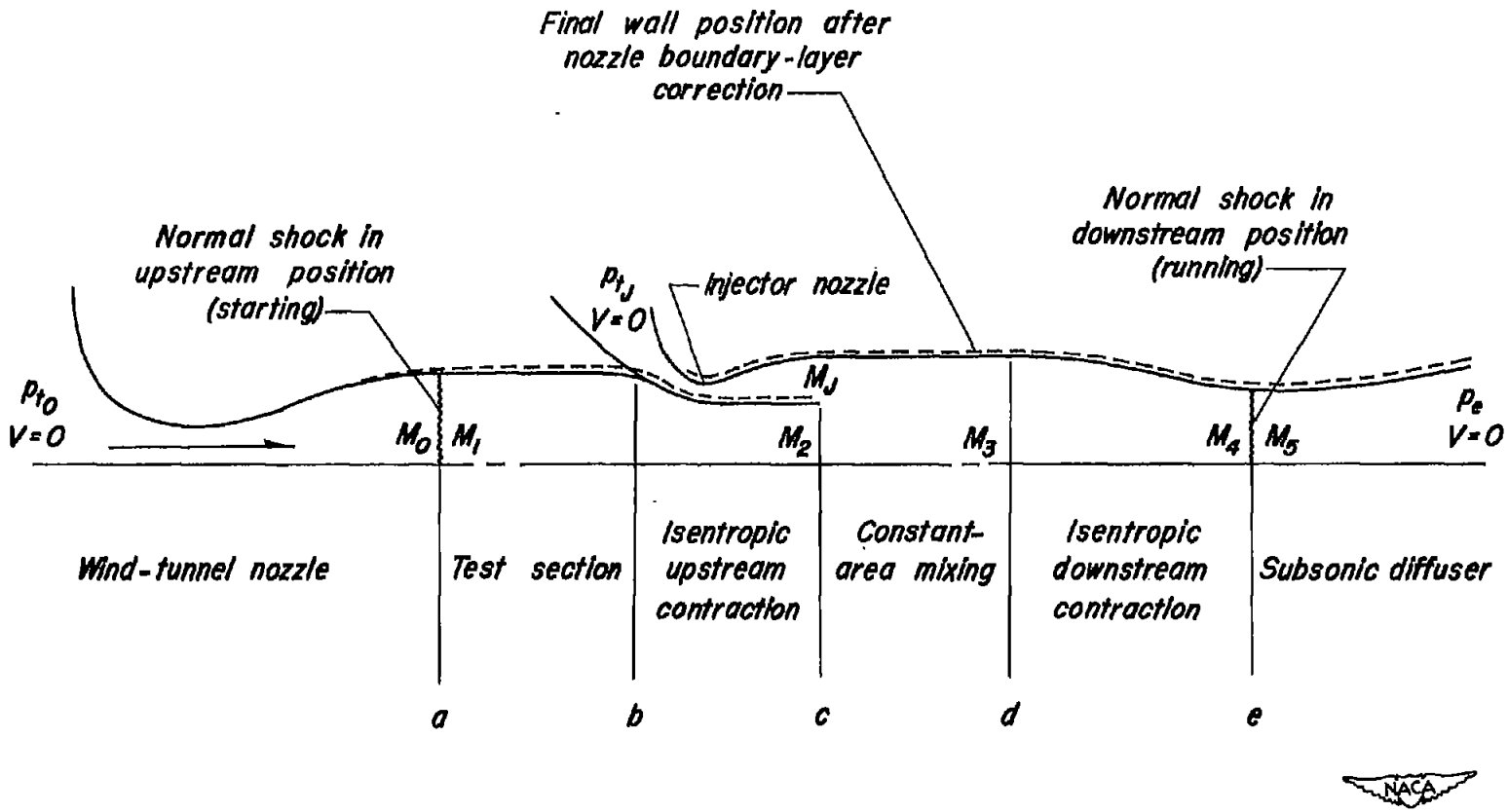

Figure 1.- Idealized arrangement of an auxiliary air injector for a supersonic wind tunnel (two-dimensional).

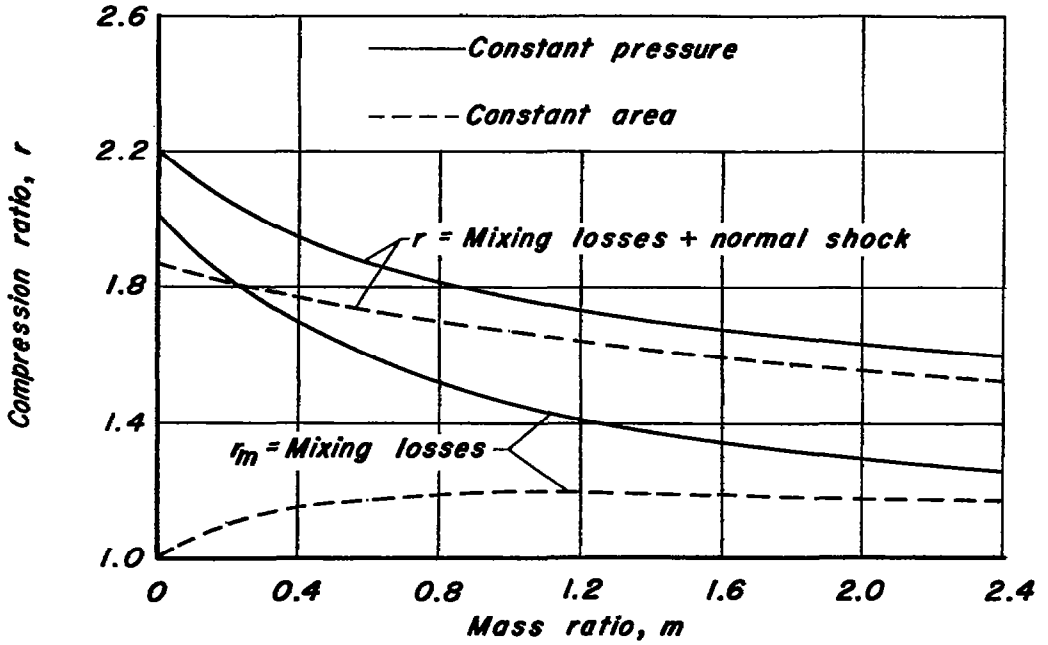

(a) Compression ratio.

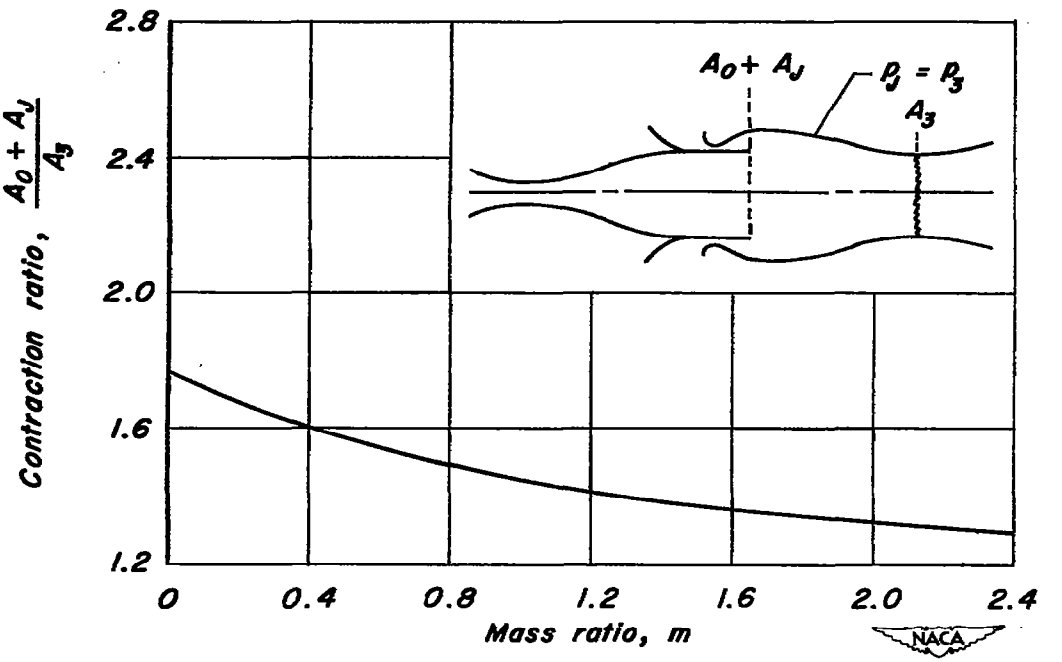

(b) Contraction ratio for constant-pressure mixing.

Figure 2.- Comparison of constant-area and constant-pressure mixing for equal areas at A_3 (running condition). $M_0 = 3$, $M_J = 2$, $K = 1$

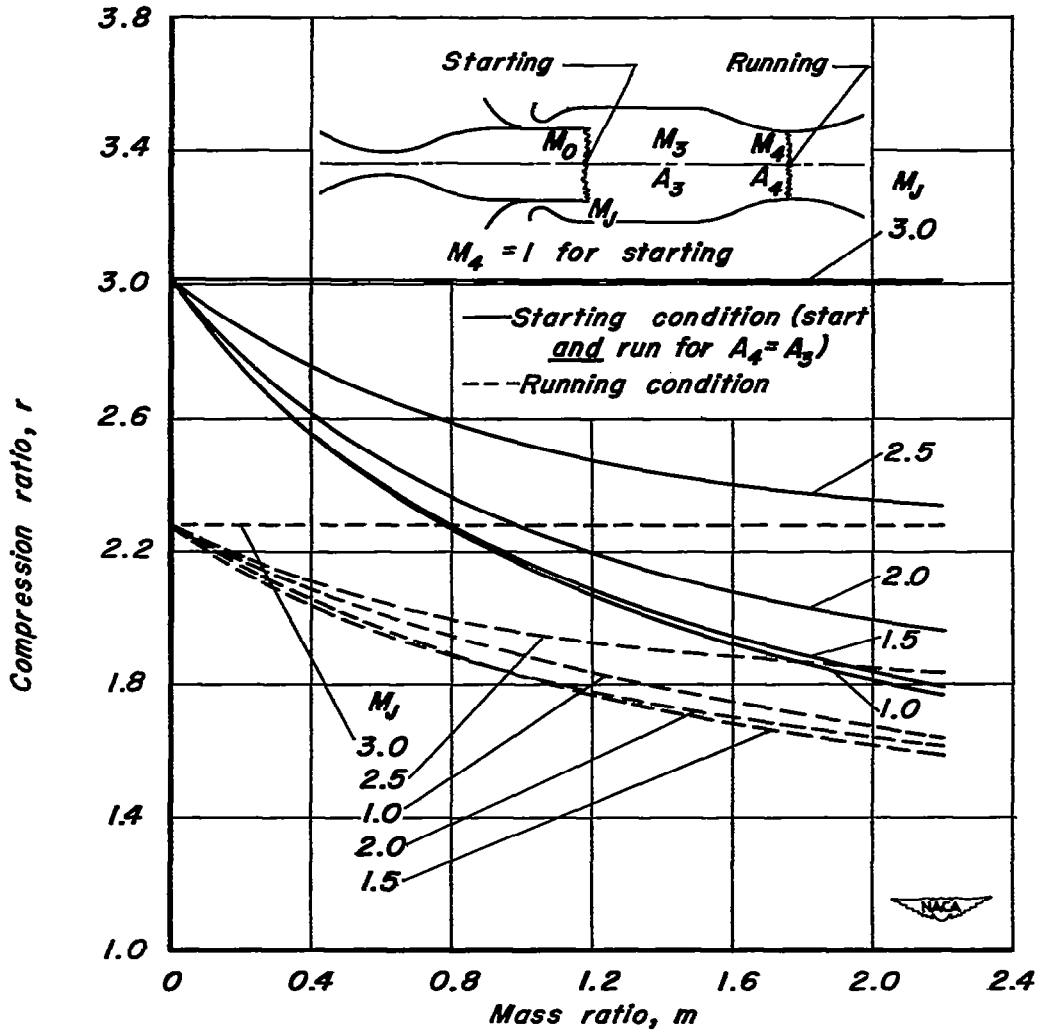

Figure 3.- Effect of injection Mach number and downstream contraction. $M_0 = 3$, $K = 1$

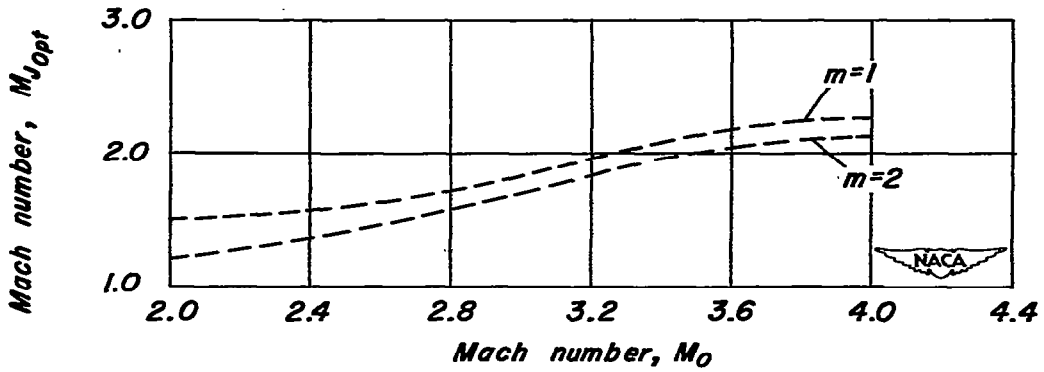

Figure 4.- Variation of optimum injection Mach number with test section Mach number (running condition). $K = 1$

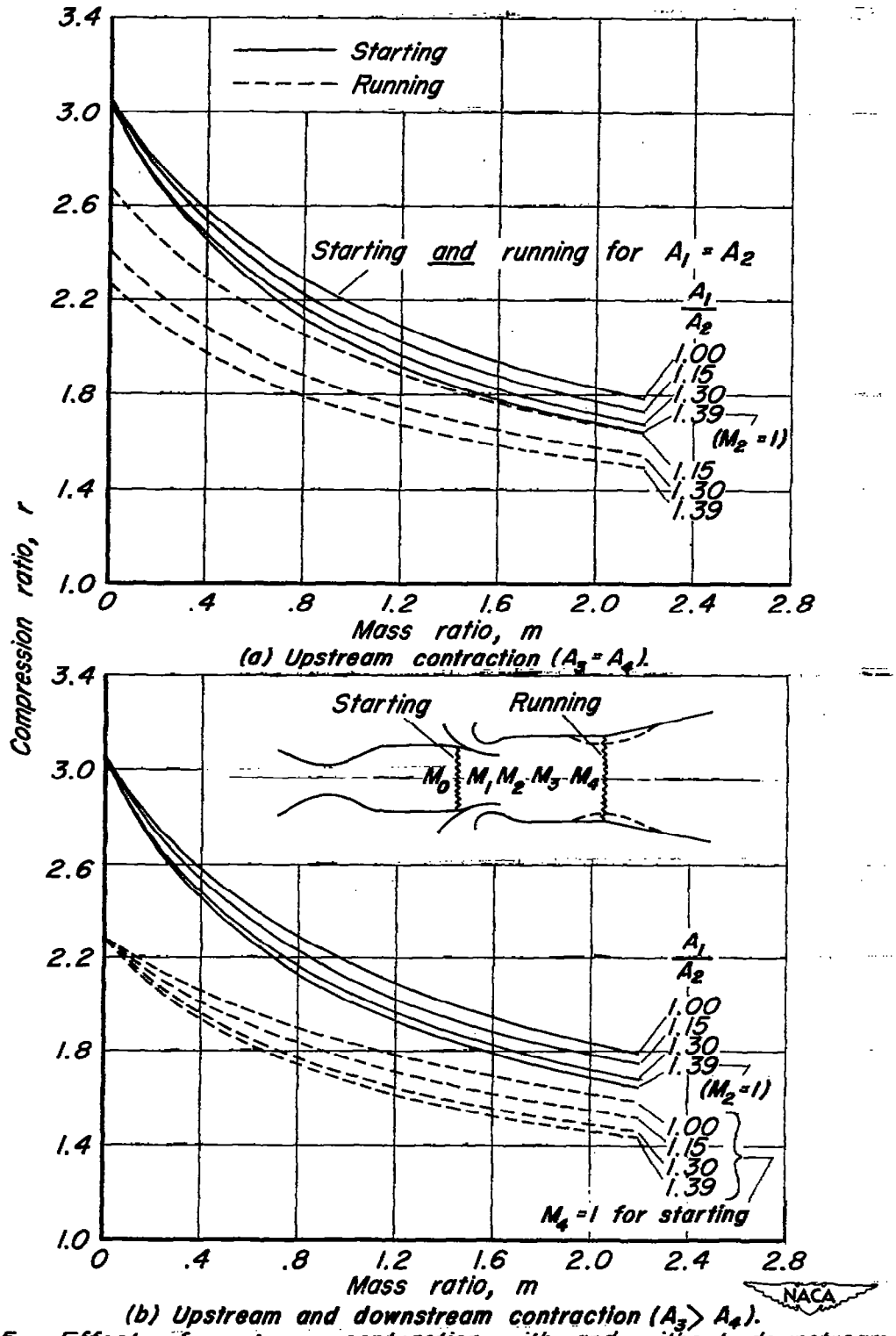

Figure 5.- Effect of upstream contraction with and without downstream contraction. $M_0 = 3.0$, $M_1 = 1.5$, $K = 1.0$

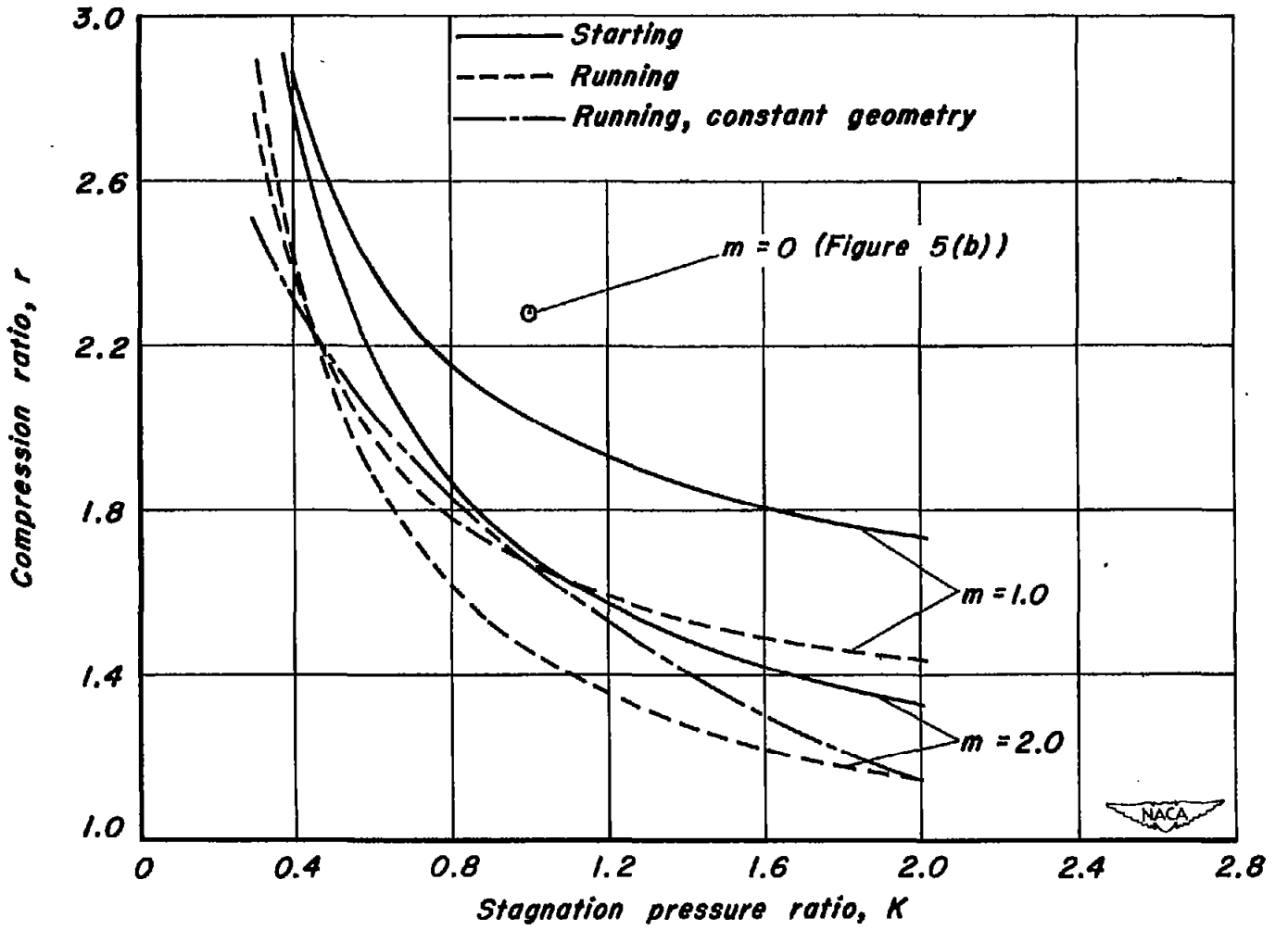

Figure 6.- Effect of stagnation pressure ratio, K. Maximum downstream contraction for starting, $M_0 = 3.0$, $M_j = 1.5$, $\frac{A_1}{A_2} = 1.39$.

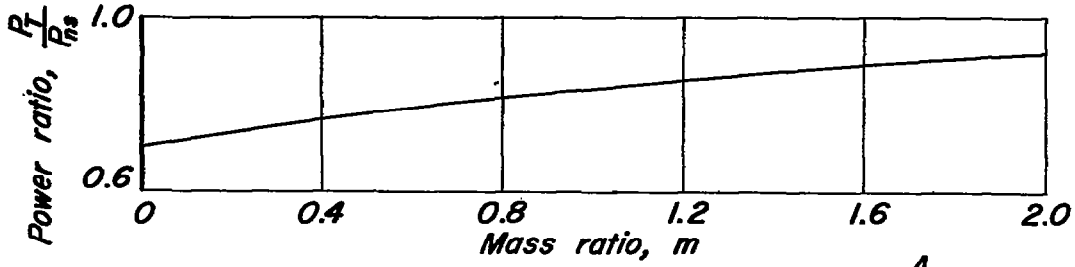

(a) Effect of m, K=1.0 (corresponds to figure 5 (b), $\frac{A_1}{A_2}$ =1.39, running condition).

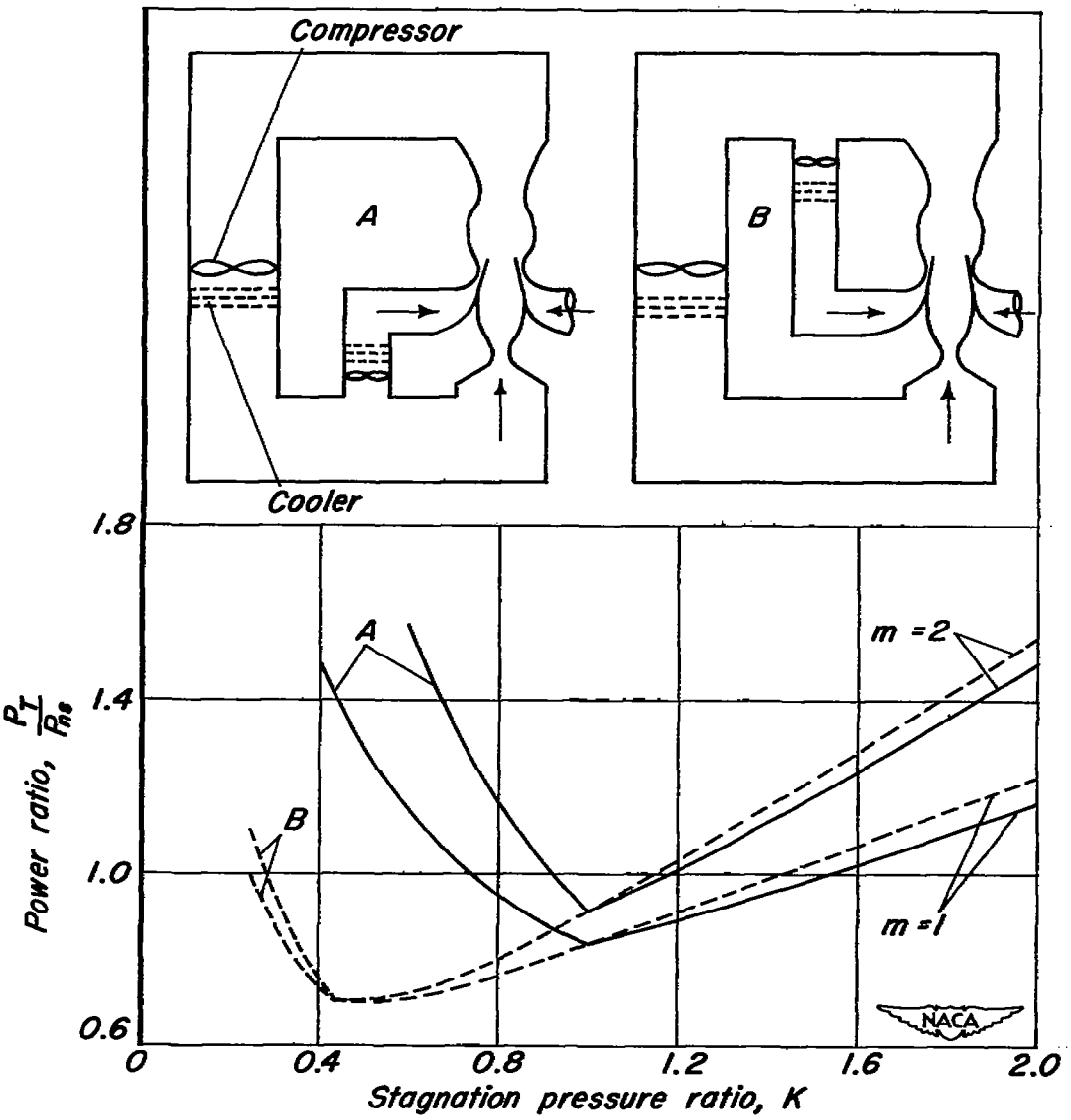

(b) Effect of K (corresponds to figure 6, running condition).

Figure 7.- Effect of auxiliary injection on total power requirements.

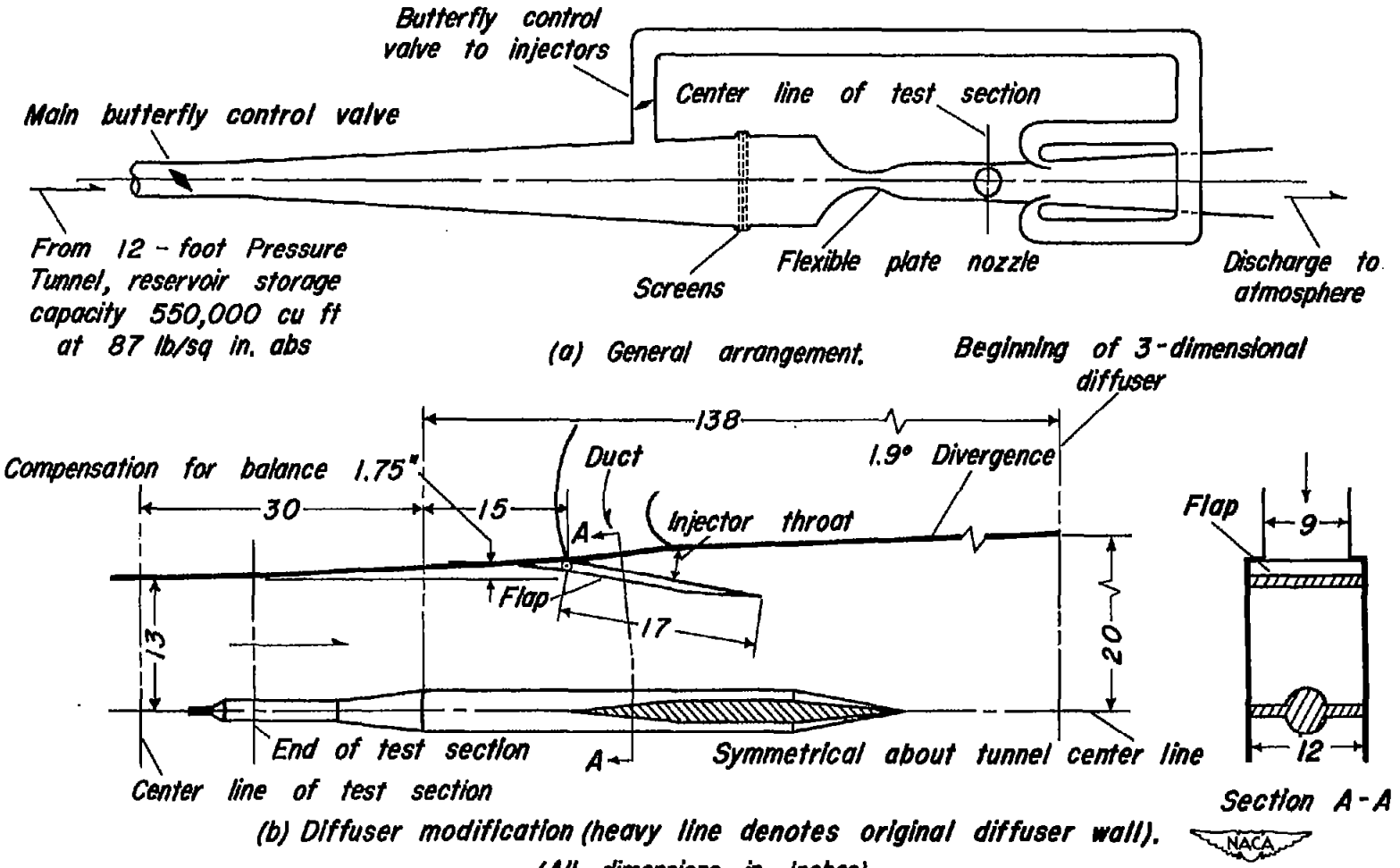

Figure 8. - Auxiliary-injector installation for the Ames 1-by 3-foot Supersonic Wind Tunnel No. 2.

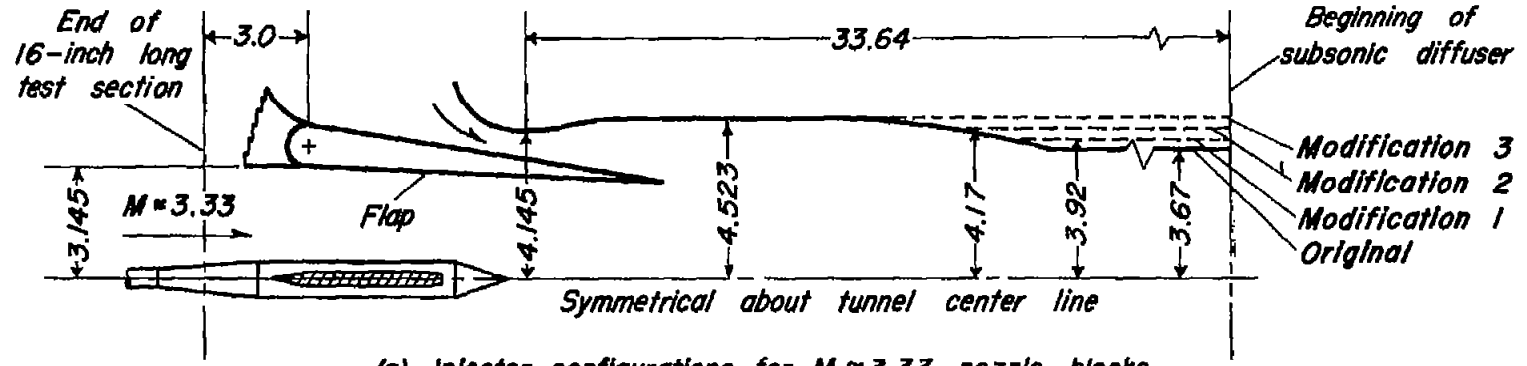

(a) Injector configurations for $M_0 = 3.33$ nozzle blocks.

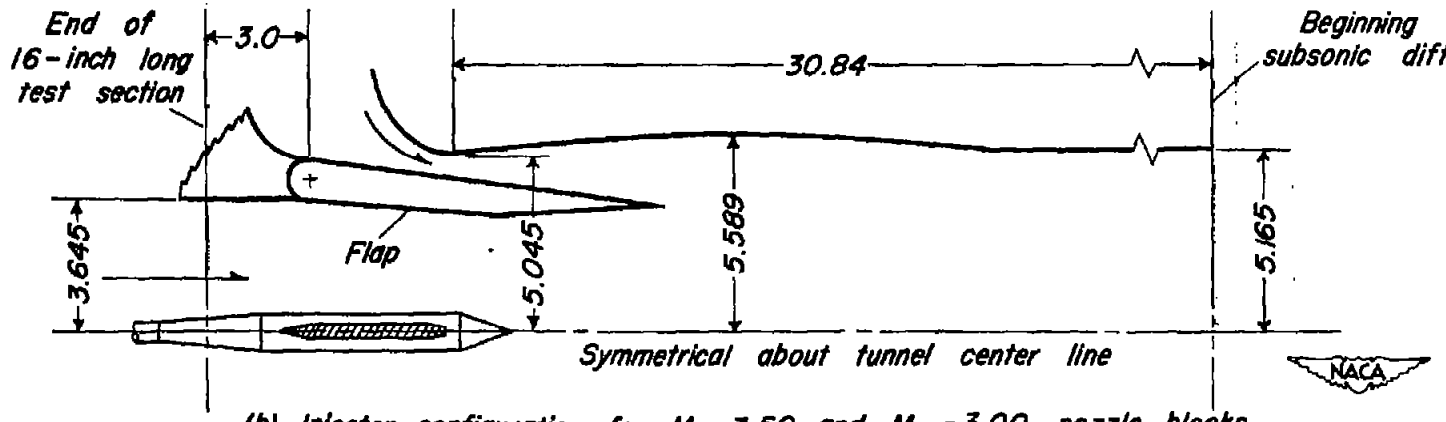

(b) Injector configuration for $M_0 = 3.50$ and $M_0 = 3.00$ nozzle blocks.

Figure 9. - Auxiliary injector installation of the 8 - by 8 - inch test facility showing the various diffuser configurations tested; Channel width = 8 inches. (All dimensions in inches)

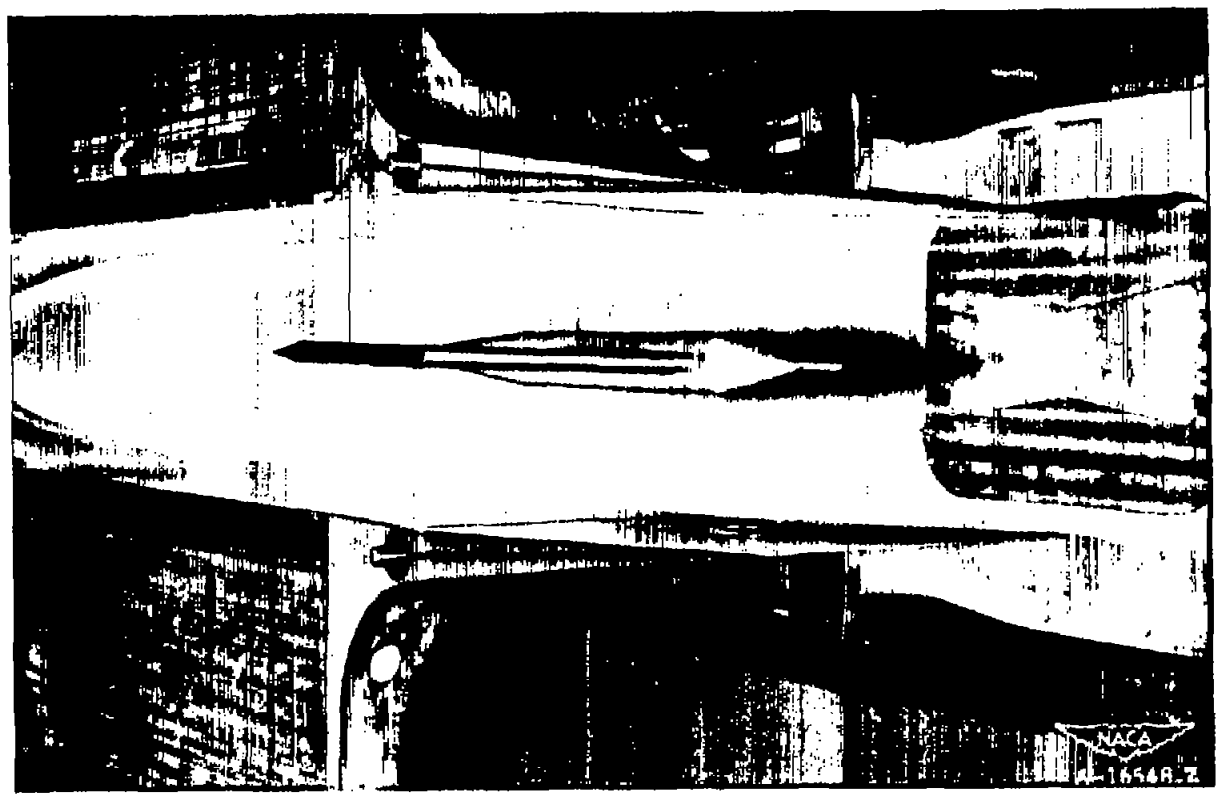

Figure 10.- Photograph of injector installation for the 8- by 8-inch test facility with one wall removed (corresponds to fig. 9(a)).

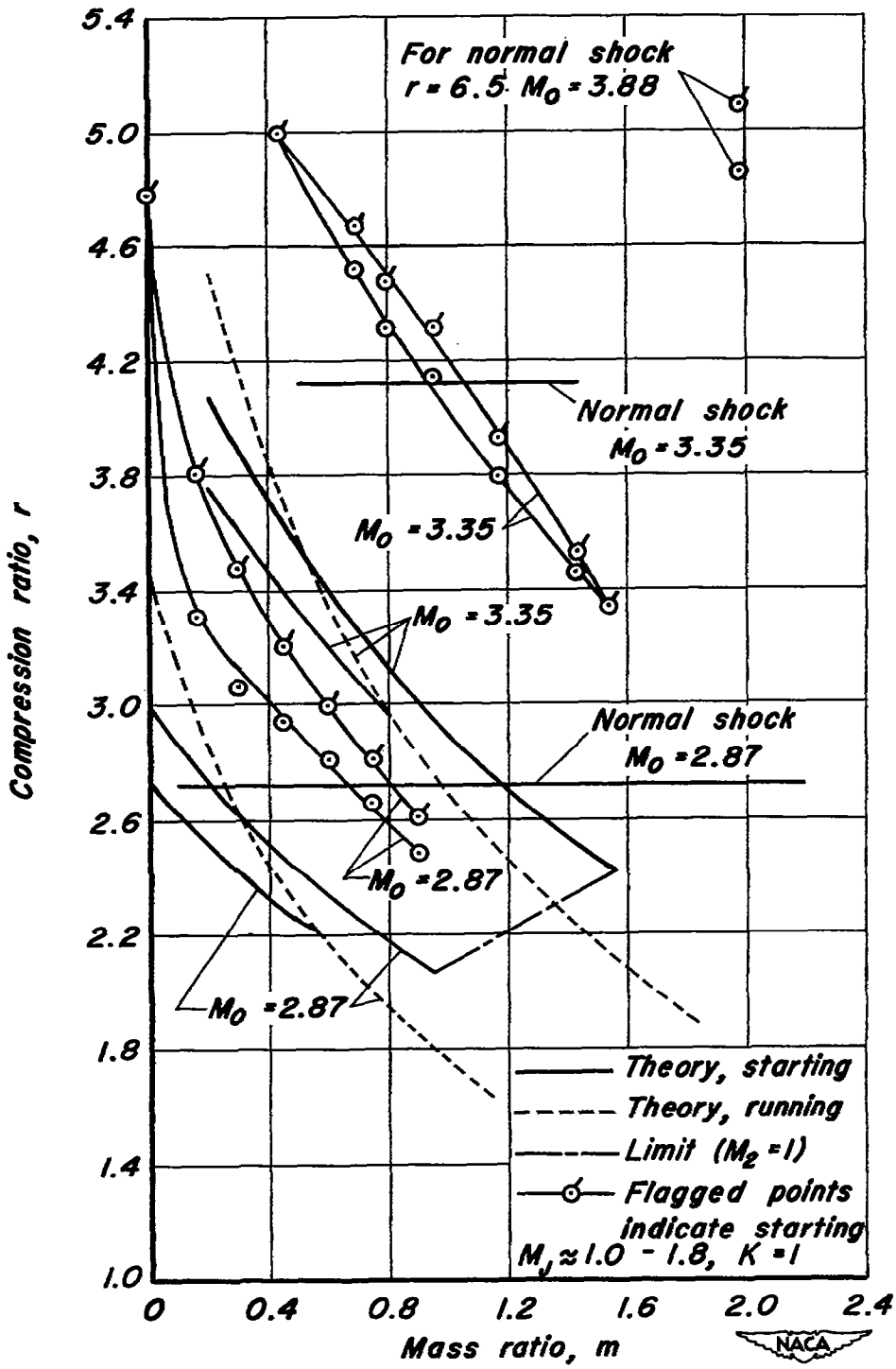

Figure 11.- Test data obtained from the Ames 1-by 3-foot Supersonic Wind Tunnel No. 2 as compared to theory.

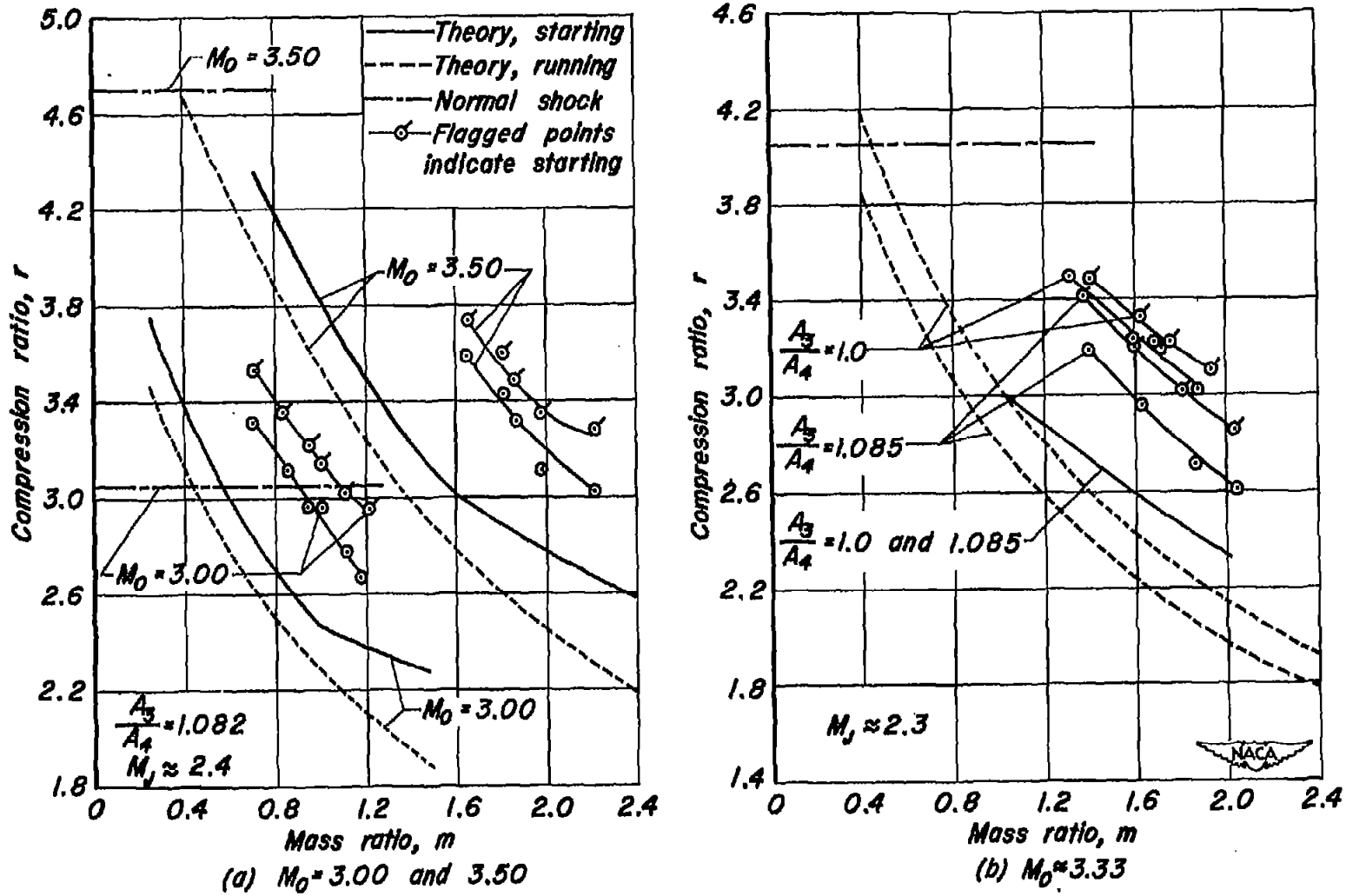

(a) M_0 = 3.00 and 3.50

(b) M_0 = 3.33

Figure 12. - Test data obtained from the 8 - by 8 - inch test facility as compared to theory. K = 1

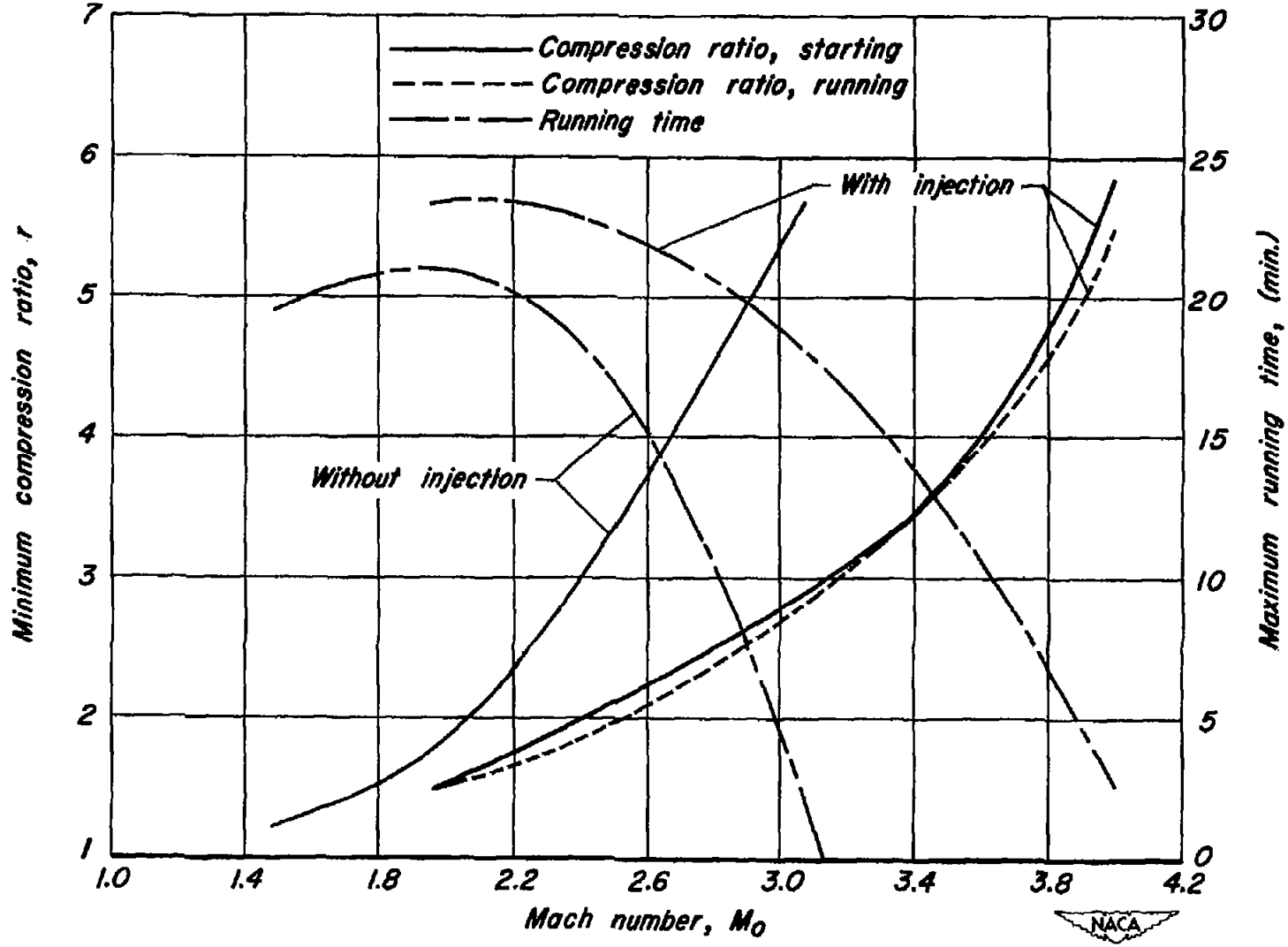

Figure 13.- Performance of 1-by 3- foot Supersonic Wind Tunnel No. 2 (blowdown tunnel) as determined from experimental data.

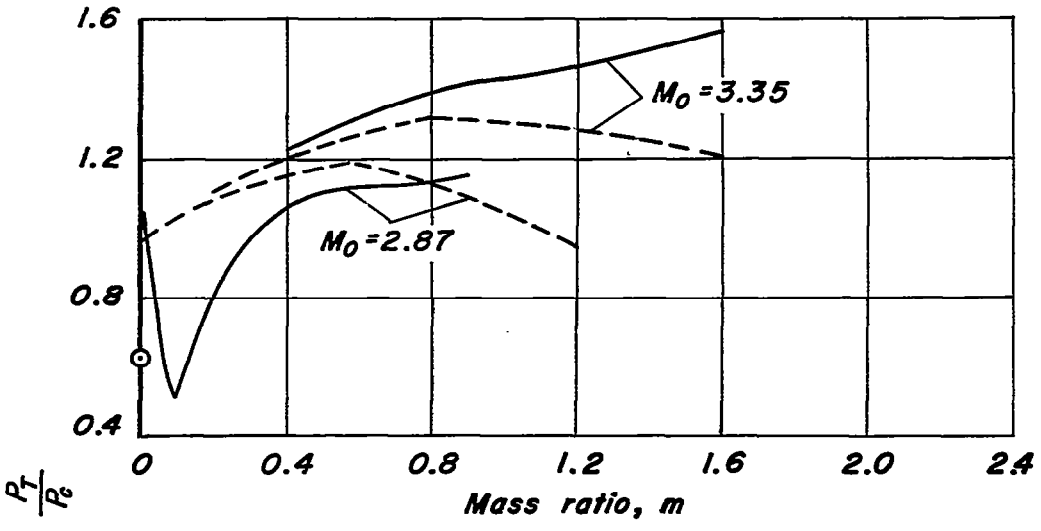

(a) 1 - by 3 - foot Supersonic Wind Tunnel No. 2.

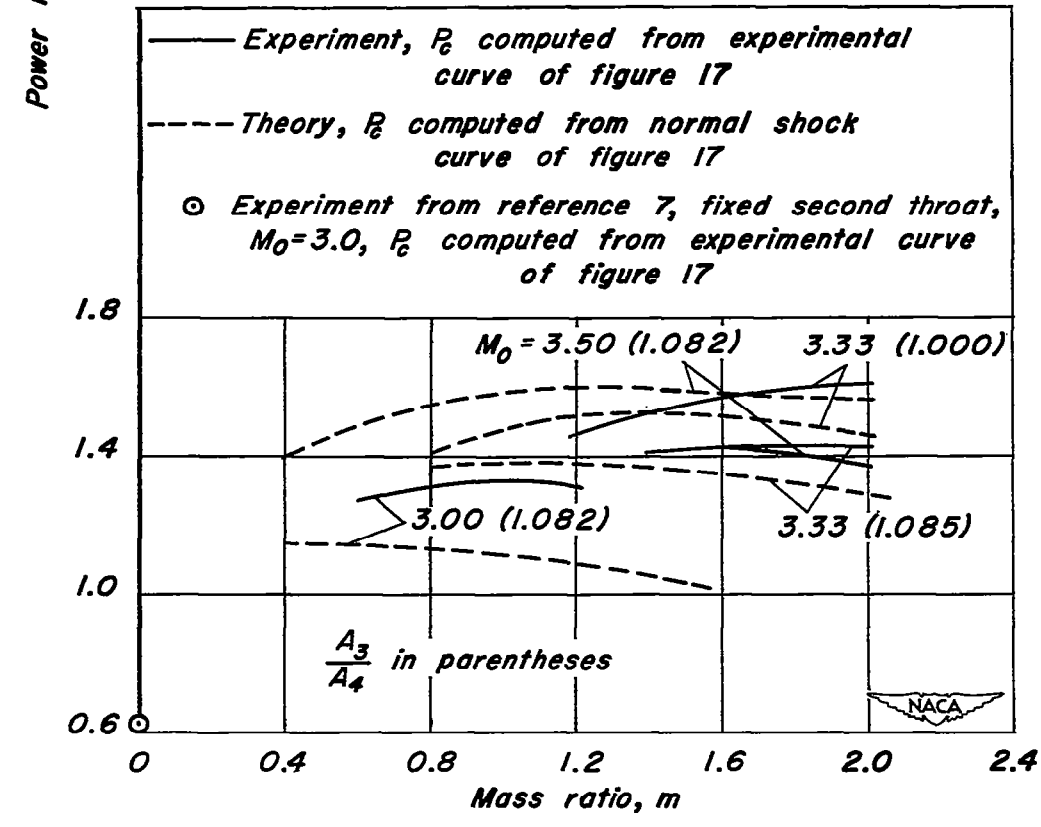

(b) 8 - by 8 - inch test facility.

Figure 14. - Effect of auxiliary injection on total power requirements of injector configurations tested.

(a) Injector off, M_o = 2.95, r = 5.27 (unsteady flow).

(b) Injector off, M_o = 2.95, r = 5.27 (unsteady flow).

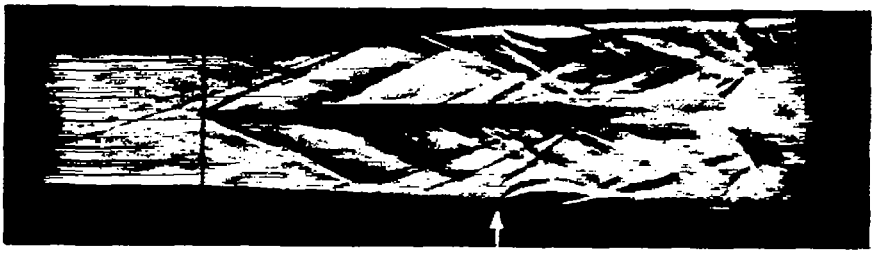

(c) Injector on, M_o = 2.95, M_J = 1.0, m = 0.40, r = 4.11 (steady flow).

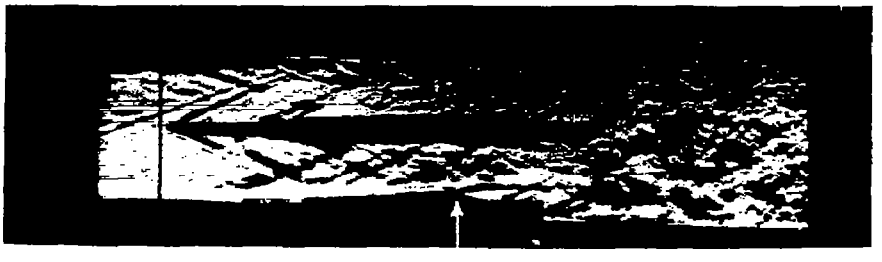

NACA A-18238

(d) Injector on, M_o = 2.95, M_J = 1.83, m = 0.60, r = 3.31 (steady flow).

Figure 15.- Schlieren pictures of the flow in the 1/12-scale model of the Ames 1- by 3-foot supersonic wind tunnel No. 2 showing some effects of auxiliary air injection. (Arrows indicate injection point.)

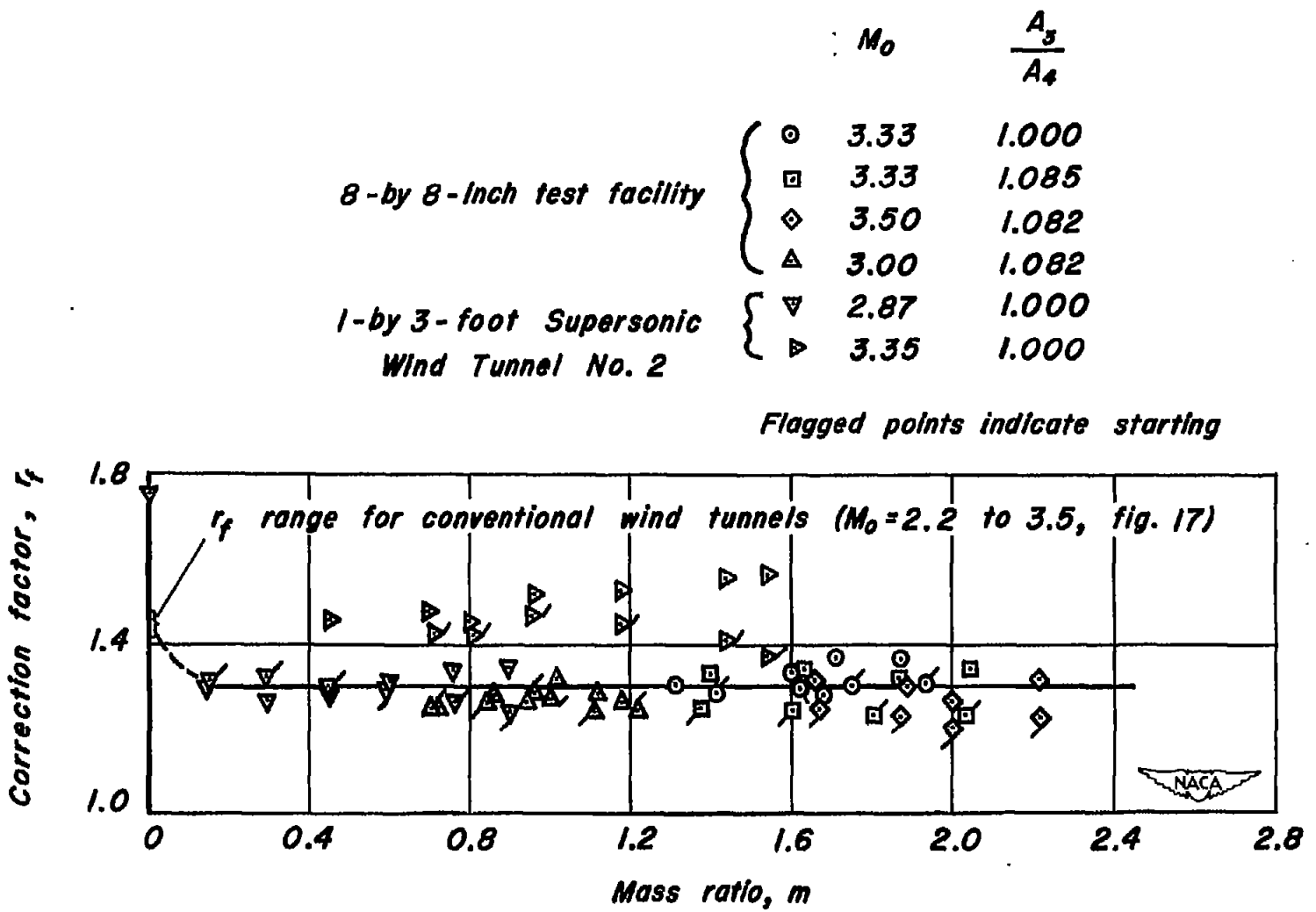

Figure 16. - A comparison of experiment to theory for two injector installations.

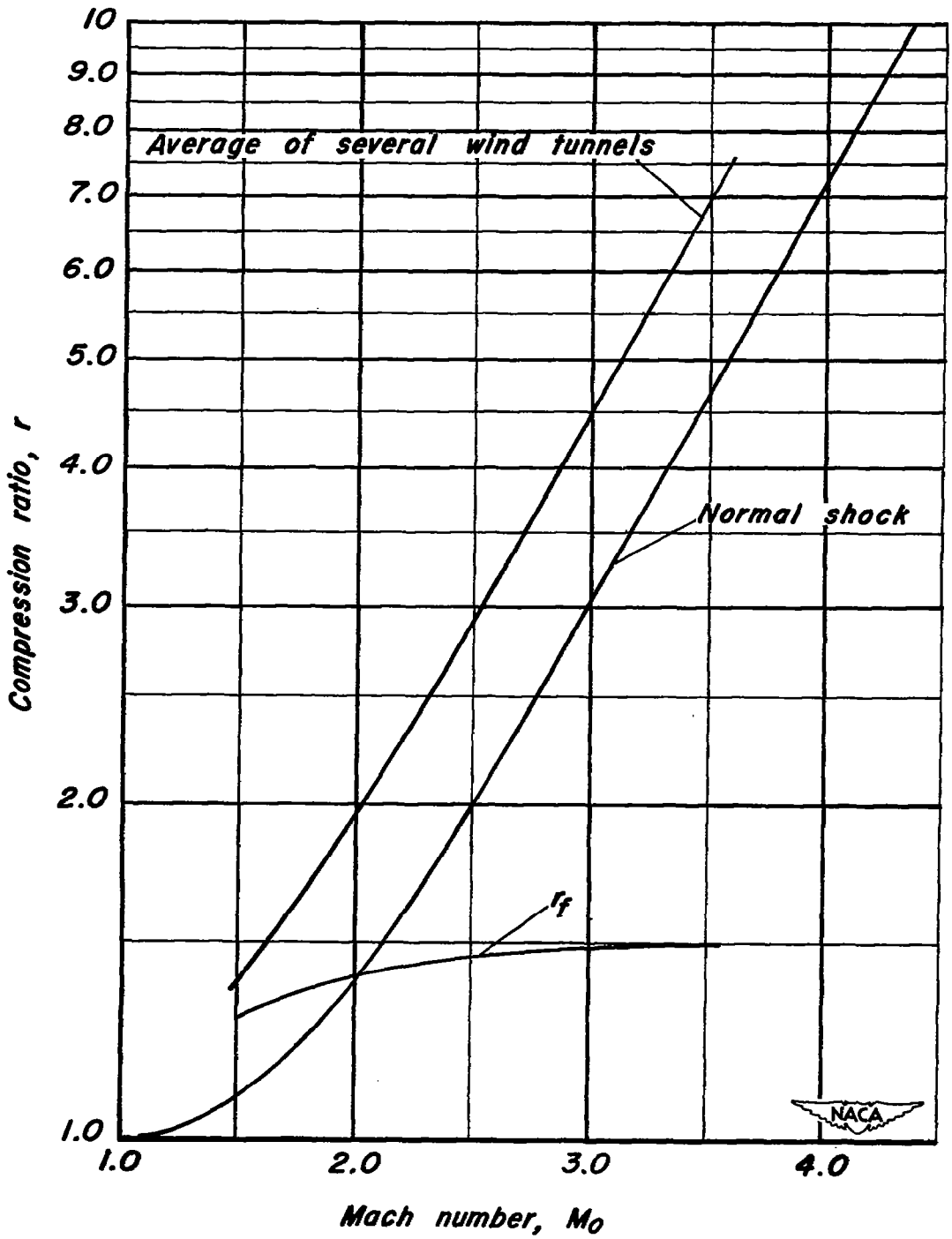

Figure 17.- Average minimum compression-ratio requirements of several conventional wind tunnels and corresponding correction factors (r_f).

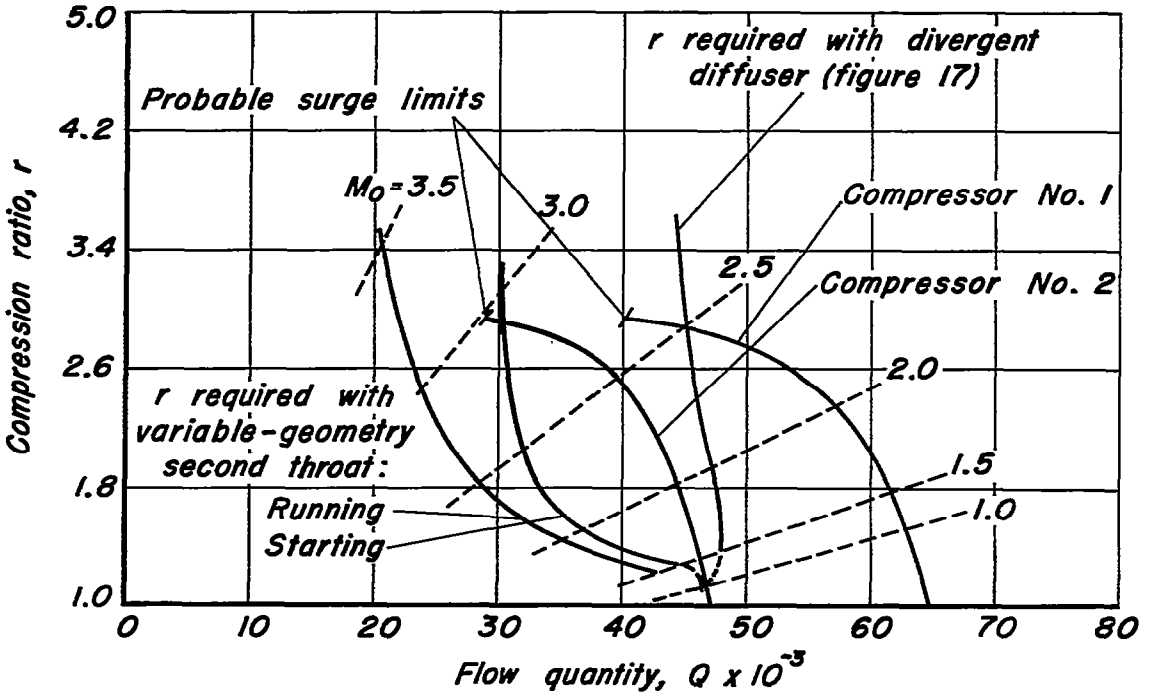

(a) No injectors.

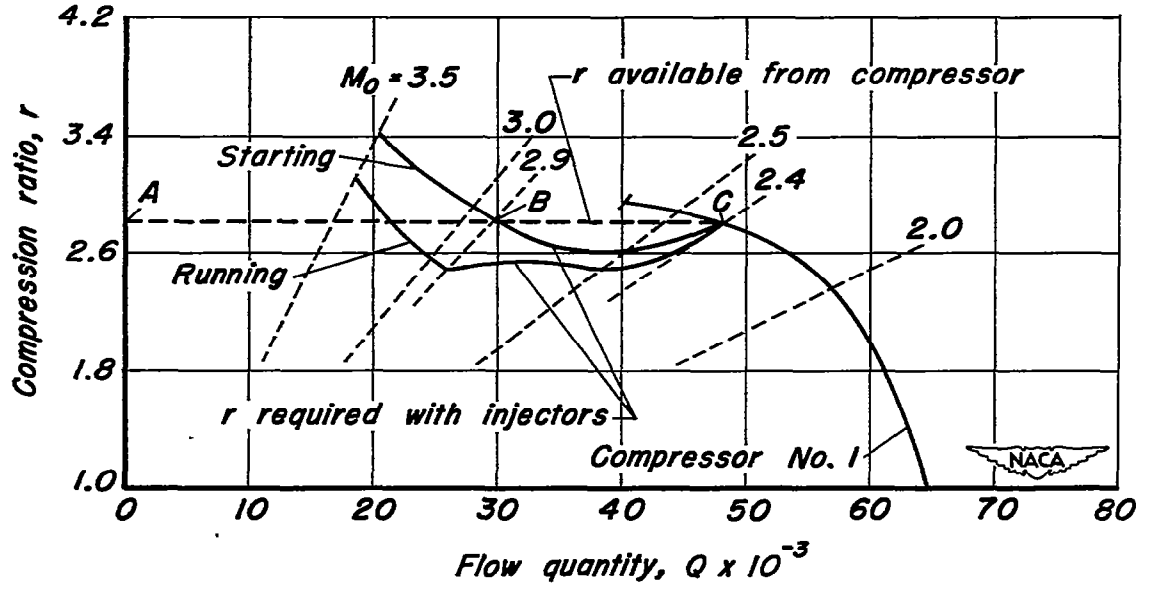

(b) With injectors, $M_j = 1.00$ to 2.29, $K = 1$, r_f included.

Figure 18.– Typical compressor and wind-tunnel diffuser performance curves.